

# Nonlinear photonics in undergraduate curriculum: hands-on training to meet the demands of a qualified workforce

Juan J. Arango<sup>a</sup>, Samuel Bechtold<sup>b</sup>, Pablo Bedoya-Ríos<sup>a</sup>, and Samuel Serna<sup>b</sup>

<sup>a</sup>School of Physics, Universidad Nacional de Colombia, A.A. 3840 Medellín, Colombia

<sup>b</sup>Department of Physics, Photonics and Optical Engineering, Bridgewater State University, Bridgewater, United States of America

## ABSTRACT

The understanding of light-matter interaction processes has been essential for the attainment of many modern advancements in photonics, for instance the telecom revolution with lasers and fiber optics. Thereby, related industries greatly benefit from large availability of professionals, qualified for undertaking projects focused on devising and scaling products that may capitalize scientific progress on photonic materials and novel optical effects. Nevertheless, the familiarity with the application of these phenomena is usually gained by scientists and engineers at graduate education level, which commonly leads to a skilled workforce shortage. This lack of photonic-capable engineers becomes more critical when discussing nonlinear and quantum applications that will be broadly available soon. With this motivation, we present a nonlinear photonics hands-on training that could be integrated into curricula for photonics engineers or material scientists. The proposed session is aimed at undergraduate students, who would develop through practical experience relevant multidisciplinary skills for experimental design, data acquisition, setup configuration and optical alignment. Manuals are provided for the implementation of Z-Scan technique in the characterization of nonlinear optical materials. Equipment requirements are included along with the undergraduate-level theoretical content that may serve as introduction for students without prior exposure to nonlinear optics. Additionally, an open-source python-based software is provided for simplifying the extraction of Kerr effect and two-photon absorption figures of merit by means of the analysis of power measurements.

**Keywords:** Nonlinear Optics, Z-scan, Undergraduate Curriculum, Hands-on Training, Photonic Materials, Optical Kerr Effect, Two-Photon Absorption

## 1. INTRODUCTION

In recent years, integrated photonics has proven itself as a promising platform for the development of complex engineering tasks demanded by the significant growth of industry interest on revolutionary technologies (e.g., quantum communications, neurophotonics, ultra-fast devices). Integrated photonics offers undisputed potential for miniaturizing large and complex optical systems, since its operation is based on light confinement within micro-metric structures. Academic and industrial efforts on integrated photonics development have allowed the attainment of remarkable performance features, such as cost-effectiveness, low loss signal transmission, multiplexing capabilities, device reliability, among others. These characteristics turn modern integrated photonic devices into realistic valuable means to meet technological demands of industries related with the dramatic growth of data centers and optical networks, 5G communications, all-optical data processing, second quantum revolution, etc.<sup>1-4</sup> In this way, there is an evidenced preference trend within optics academic community and related industry for integrated platforms for the execution of experiments and the development of applications that require complex optical setups and strict standards of reproducibility, such as quantum teleportation,<sup>5</sup> boson sampling,<sup>6</sup> or all-optical switches.<sup>7</sup> Likewise, applications such as high-dimensional quantum information processors<sup>8-10</sup> and coherent integrated light sources could be directly studied and developed on photonic chips, which are fields of active research.<sup>3</sup> Recent technological road-maps,<sup>1-4</sup> on different specific applications,

---

Further author information: (Send correspondence to J.J.A.)

J.J.A.: E-mail: [jujarangour@unal.edu.co](mailto:jujarangour@unal.edu.co), Telephone: +57 604 430 9327

S.S.: E-mail: [ssernaotalvaro@bridgew.edu](mailto:ssernaotalvaro@bridgew.edu), Telephone: +1 508 531 2040

have also pointed out integrated photonics as the platform of choice for multiple future technologies, but have emphasized in the need of a well trained workforce to make it work, urging for the establishment of education initiatives for the training of professionals and technicians with specialized knowledge and extensive hands-on experience on integrated photonics methods and techniques.<sup>1</sup> Accordingly, national initiatives in the United States, as AIM Photonics<sup>11</sup> (American Institute for Manufacturing Integrated Photonics) and the National Photonics Initiative,<sup>12</sup> are intensely working on the growth of photonics from innovation to manufacturing systems for novel technologies, claiming that photonics should be a national priority. There is emphasis on the importance of the industrialization of photonics,<sup>13</sup> and the recruitment of qualified workforce for different manufacturing careers.<sup>14</sup> Furthermore, there are federal programs that encourage the development of photonics. For example, in the state of Massachusetts, MassTech provides funding for different photonics initiatives.<sup>15</sup> As photonics is a promising platform for the development of emerging technologies, others initiatives, as the National Quantum Initiative,<sup>16</sup> also promote the use of photonics for the implementation and deployment of quantum computing services, quantum networks, and cybersecurity schemes. All this funding and public/private initiatives are supporting the diversification and consolidation of new and traditional industries, which in turn put more pressure on the currently limited specialized labour market.<sup>17</sup>

Along with integrated photonics comes nonlinear optics,<sup>18</sup> as the confinement of light in micrometric structures intensifies the light-matter interaction processes that lead to nonlinear phenomena. With the invention of the laser, many applications that rely on intense light have arisen, and their development has been supported on nonlinear optics. In this way, progress on coherent light sources construction, quantum entanglement generation, all-optical signal processing, spectroscopy, telecommunications, and computing has leveraged the accumulated knowledge and techniques in nonlinear optics,<sup>19</sup> and should be part of modern curricular proposals, accessible for those undergraduate students interested in advanced courses and research exposure. The importance of undergraduate research has been highlighted,<sup>20</sup> as it provides the opportunity for the students to understand the research process from an early stage of their careers, and to develop advanced skills such as laboratory techniques and results interpretation, among other important skills required by both academic and industrial employers. Unfortunately, nonlinear optics is a subject that is commonly approached at postgraduate level, and it is usually not studied in depth in regular undergraduate STEM programs. Therefore, including hands-on training in nonlinear photonics in the undergraduate STEM curricula is identified as a challenging but necessary curricular reform, in the view of the fact that a qualified workforce is required by the emerging and growing industries in this area.

In this work we discuss the set of skills that should be included in an up-to-date responsive curriculum in section 2. And, as illustration of the novel pedagogical strategies that should be introduced, we propose a laboratory practice centered on the implementation of the Z-Scan technique, arguing why such educational activities may be a suitable way of training the workforce for future photonic labour market. So, in section 3, we summarize the expected results of the proposed Z-Scan implementation, taking the experience in Bridgewater State University undergraduate laboratories as study case. Furthermore, Appendix A provides a theoretical introduction to nonlinear optics, and a detailed experimental manual for the proposed laboratory practice; and Appendix B explains the proposed methodologies for data processing and material properties determination, by means of the use of an open-source software that was developed by our team. It is expected that the educational resources provided in Appendices A and B will result very helpful for institutions and instructors commissioned with the development or modernization of related educational programs.

## 2. CURRICULUM CONTENT FOR A QUALIFIED WORKFORCE

Given the current requirements of the optics and photonics industry, professionals will find challenges in different areas of knowledge as: physical phenomena modeling, experiments design, data acquisition, data processing, and optical equipment handling. Thus, any curricular proposal seeking to train professionals in the area of photonics should provide resources for their development.

In this work we propose a laboratory practice for undergraduate students, that gathers learning opportunities in all aforementioned areas, consisting in the implementation of the Z-Scan technique<sup>21</sup> for nonlinear materials characterization. The Z-Scan technique may be described as follows: A sample is placed after a lens and before a detector, whose detection are may be restricted by a blocking element. The lens is illuminated by high intensity

light, which is detected after the focal plane of the lens by a power meter. Thus, the intensity detected at the detector plane will depend on the convergence and divergence of the optical system composed by the lens and the sample. This means, that the intensity at the detector plane will depend on the position of the sample, which commonly is located along the  $z$ -axis, hence the name "Z-Scan". This means that the optical properties of the sample are changing due the intense electric field of the light that is illuminating the sample. In this specific case these changes are associated to the nonlinear refractive index of the material,  $n_2$ , and its two-photon absorption coefficient,  $\beta_{TPA}$ . These are the parameters that the technique implementation allows to determine. Given this, during the laboratory practice, students learn the basics of optical equipment handling, as they are required to build the setup for the Z-Scan technique. The students must model the physical phenomena occurring during the experiment, in order to know and understand which variables should be measured. The students must know experimental design, to find the possible statistical error sources and take them into consideration in the final calculations. And students must develop as well skills for the appropriate data acquisition and interpretation, in order to obtain accurate results. Knowing this, an implementation of the Z-Scan technique comprises a valuable training activity for undergraduate students, as it entails challenges that are common in the photonics industry and academia. It is worth saying that not long ago, the Z-Scan technique could only be implemented by selected laboratories with specialized equipment. Now, the equipment is more accessible and affordable,<sup>22-24</sup> even in the market there are kits that include all the necessary items for a reasonable price. The main equipment needed for the Z-Scan implementation comprises the following: a high-power laser, and multiple conventional table-top optical elements, that may vary depending on how the optical system will be formed; namely, lens, half-wave plates, quarter-wave plates, beam splitters, and mirrors. All of them with their respective mounts. They are also needed a prepared mounted sample, an optical aperture, an optical power-meter, and data acquisition electronics. The most relevant considerations for the setup design are discussed below.

- **High-Power laser:** The laser can be continuous-wave (CW) or pulsed, the requirement is that the power is high enough to excite the nonlinearities of the sample. It should be noticed that for more accurate results, the selection of laser light intensity depends on the thickness of the sample,<sup>25</sup> and if CW lasers or pulsed lasers with long pulse duration are preferred, the potential excitation of thermal optical nonlinearities must be taken into consideration.
- **Optical Elements:** There are many ways of building the experimental setup to implement the Z-Scan technique. Depending on the laser, the detectors and the experimental protocol some filters should be used for controlled optical attenuation. Also, if  $n_2$  and  $\beta_{TPA}$  should be measured simultaneously, some additional elements may be require for signal sampling. For example, in our implementation (see section A.3) we used: a plano-convex spherical lens, several mirrors for facilitating optical alignment, and a rotating half-wave plate with a polarizing beamsplitter to control light polarization state and incident power level. It is worth mentioning that for measuring nonlinearities in crystals it is important to keep track of the polarization state of laser light, and its relative orientation with crystal's lattice.
- **Prepared Mounted Sample:** If solid crystals or glasses are characterized, their mounting is usually simple, and the sample preparation depends on the material synthesis method. The characterization of solids is usually made by direct exposition of the sample to the laser radiation. If liquids or gases are characterized, specialized cuvettes or chambers would be required. In these cases, properties of the walls of the cuvette or chamber that get exposed to the radiation must be taken into consideration in the experimental protocol, in order to compensate the effect that these external objects might have in the optical power detection. Strict control of the thermodynamic conditions of liquids or gases may also be crucial for accurate experimental results.
- **Optical Power-Meter:** When implementing the Z-Scan technique, two kinds of measurement are needed: closed-aperture and open-aperture (for more details see Appendix A). There are implementation strategies that allow for their simultaneous measurement. In these cases, it is necessary to have two power meters or a dual power meter. Before making a choice on the power-meters to be used, it is important to take into consideration the supported power scales ranges, and the corresponding resolution values; since the inappropriate selection of the power-meter may result in the saturation of the sensor, very low signal-to-noise ratio, or imperceptible variations of the detected signal.

- **Electronics:** The data collected by the power-meter(s) has to be processed to infer the nonlinear properties of the material under study. Thus, it has to be transferred from the power meter(s) to a computerized system. Some power-meters have integrated software that will perform the direct conversion from electrical to optical variables. In other cases, optical power measurement has to be obtained from current or voltage direct measurements.

It is worth noting that, by investing in having these kind of experimental practices available for undergraduate programs, not only learning and training spaces are offered to students, but also undergraduate research opportunities are unleashed. As evidence it is shown that this simple methodology enables the measurement of scientifically relevant quantities, such as the two-photon absorption coefficient and the nonlinear refractive index.

### 3. EXPECTED RESULTS OF THE IMPLEMENTATION OF THE Z-SCAN

At Bridgewater State University (BSU), undergraduate students have the opportunity to perform Z-Scan measurements with the equipment in the recently established Photonics Laboratory. The experimental setup is fully installed, allowing students to utilize this experimental setup for the measurement of thin-film materials that have been sent to the lab for study. Students first must undergo standard training on the experimental procedures, including sample preparation. This gives students the opportunity to work with academic and industry partners who rely on the Photonics Lab for the characterization of their submitted materials. To prepare samples for a Z-Scan, students must take care not to damage the samples by wearing gloves and ensuring no other materials touch the sample. Cleaning of dust is accomplished with air spray canisters as to not leave material traces on the sample. Once cleaned the samples are carefully attached to a mount and then placed onto the translation stage for the Z-Scan. Once the sample is mounted, students must then turn on the laser system and use a viewing card to ensure the system is aligned properly. The measurement scheme for the Z-Scan must be precise (with enough data points to ensure the resolution of the resulting graph is high enough to see the expected patterns for the Z-Scans). This measurement scheme must also be repeated for each Z-Scan, therefore the process requires the student to measure the input power of the system before the focusing lens that lies before the sample. This measurement should be standard for each Z-Scan, with another standard power measurement for the closed aperture scan (the aperture lying after the translation stage) to ensure the same aperture radius is used for each Z-Scan. Once the setup measurements are made, the student must ensure the translation stage is adjusted to the zero position and that the power meter is connected to a computer with the the optical power monitor software on. This software allows students to focus on precise movements of the translation stage between measurements while the program takes automatic measurements at a set time interval, allowing for the Z-Scan procedure to be carried out by one operator, rather than two. This also drastically reduces the length of a Z-Scan measurement. All the details about the experimental procedures, and a introductory theoretical presentation of the related concepts, are included in the Appendix A. Additionally, students can utilize the resources in Appendix B for the extraction of the Two-Photon Absorption and Kerr nonlinearity coefficients from the data.

As an illustration of the successful execution of nonlinear materials characterization, performed by undergraduate students at BSU using the Z-Scan technique, the experimental results obtained for a silicon sample are presented in Table 1. These parameters were extracted from the experimental data presented in Fig. 17, using the open-source python script described in Appendix B, and published along with this proceeding.<sup>26</sup> Measurements were performed with incident average power values between 38 and 123 mW, with a silicon sample with a width of 350  $\mu\text{m}$ , using a pulsed laser source with a pulse duration of 90 fs and a repetition rate of 100 MHz. Results obtained are close to those reported for silicon in the academic literature.<sup>27</sup>

Table 1. Experimental results

Material	Silicon
$\beta_{TPA}$	$24.6 \times 10^{-12} \text{ m/W}$
$n_2$	$5.69 \times 10^{-18} \text{ m}^2/\text{W}$
$w_0$	19.3 $\mu\text{m}$

# APPENDIX A. UNDERGRADUATE LABORATORY PRACTICE MANUAL: Z-SCAN TECHNIQUE

## A.1 BACKGROUND

### A.1.1 Nonlinear Optics

Nonlinear optics is the area of photonics that studies the phenomena that occur as a consequence of the modification of the optical properties of a material by the presence of light.<sup>28</sup> This nonlinear behavior in photonic materials becomes measurable as a result of strong light-matter interaction processes, whose phenomenology may be explained with a simple model of a harmonic oscillator, as the one depicted in Fig. 1.

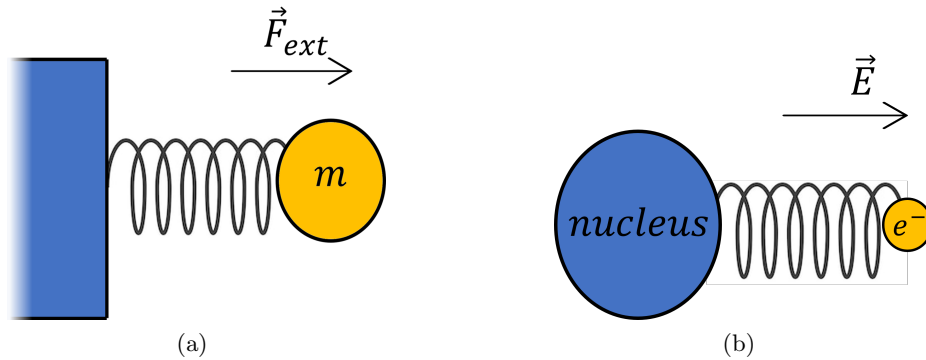


Figure 1. Conceptual sketch of (a) a harmonic oscillator based on a spring, where  $\vec{F}_{ext}$  represents an external force that is applied to the mass  $m$ , and (b) the analogous description of the dynamics of bound electrons within an atom as a harmonic oscillator with restoring forces provided by atomic electric fields, and under the influence of incident light wave with amplitude  $\vec{E}$ .

Let's suppose that in the mass-spring system from Fig. 1(a)  $\vec{F}_{ext} = 0$ , and then the mass  $m$  gets slightly disturbed. The mass  $m$  would begin to describe a simple harmonic motion. Assuming that the direction of oscillation is the horizontal axis  $x$ , the motion will be described by:

$$\ddot{x} + \omega^2 x = 0. \tag{1}$$

Next, an external force  $\vec{F}_{ext}$  is applied to  $m$ . Hooke's law,  $|\vec{F}_{res}| = -kx$ , with  $k$  the elastic constant of the string and  $x$  the strain, states that the spring exerts a force on the mass that is proportional to the elongation

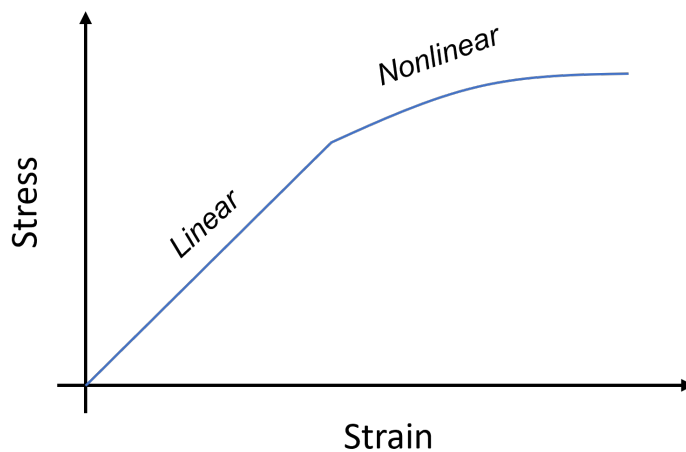


Figure 2. Conceptual graph of the Young modulus of a string. In the linear zone Hooke's law can be applied to the system. In the nonlinear zone a polynomial series expansion must be used to model the restorative force.

of the spring, as long as the strain provoked by the external force on the string remains in the linear zone of the Young modulus of the string material, Fig. 2. If the force is strong enough to deform the string through the nonlinear zone of the Young modulus, Hooke's law cannot be longer applied to model the motion dynamics, and the restorative force  $|\vec{F}_{res}|$  must be described as a polynomial series expansion, this is

$$|\vec{F}_{res}| = kx + a'x^2 + b'x^3 + \dots \quad (2)$$

Given this new restoring force formulation, the motion of the string can no longer be described by Eq. (1). Using Eq. (2), the new equation of motion for the spring-mass system under strong external perturbations is:

$$\ddot{x} + \omega^2 x + ax^2 + bx^3 + \dots = -\vec{F}_{ext}/m, \quad (3)$$

which happens to be an anharmonic oscillator, where  $a, b, \dots$  are related to the new frequencies at which the string oscillates and are closely related with the strength of the external force and the string material. The generation of new frequencies of oscillation will depend on the strength of the external force; and for a stronger force, the generation of new frequencies gets encouraged. The distribution of new frequencies that are generated depends mostly on the spring, as there are springs that are more likely to oscillate at certain frequencies than others under these extreme conditions.

Taking the dynamics of this mechanical system as reference, the interaction between an electric field and atoms could be understood as an analogous phenomenon (see Fig. 1(b)). In this case, the mass of the nucleus of each atom is much bigger than the mass of its electrons, it can be assumed that the nucleus stays still and the electrons get accelerated, driven by the incident optical field. When there is no external field, i.e.  $\vec{E} = 0$ , the atom will behave like a harmonic oscillator, the electrons will move due the attractive and repulsive forces with the nucleus and other electrons, but they are confined in the vicinity of the atom. Now, when the electric field is applied, if it is strong enough, the oscillation of the electron will follow similar dynamics as those experienced by the mechanical oscillator in Fig. 1(a). So, it would enter in a nonlinear regime, where the motion is now modeled by an anharmonic oscillator. So, the corresponding classical equation of motion is given by:

$$\ddot{x} + \omega^2 x + ax^2 + bx^3 + \dots = -eE(t)\vec{m}_e, \quad (4)$$

where  $e$  is the charge of the electron and  $m_e$  is its mass. Given the existence of an external electric field, the system will oscillate at different frequencies, when the field is strong enough. These frequencies are closely related with the terms  $ax^2 + bx^3 + \dots$ , which are nonlinear terms. In this case, the distribution of new frequencies that can be generated depends on the atom, certain atoms can oscillate at certain frequencies and others cannot. This analogy shows that the light-matter interaction for sufficiently intense optical fields involves the contribution of nonlinear terms that are related with the generation of new frequencies, giving sense to the name of the subject that studies these optical phenomena: "nonlinear optics". When the the field is not sufficiently intense, the generation of new frequencies is negligible, and the ongoing optical phenomena would belong to the "linear optics" field. Although this analogy provides a first approach to the study of nonlinear optics, for a consistent comprehensive description, more sophisticated models are required, harnessing electrodynamics and quantum mechanics principles.<sup>28</sup>

In the next section an introduction to the electromagnetic formalism used to explain nonlinear optics is given, elaborating on the nonlinear behavior of the polarization vector for susceptible materials. Additionally, nonlinear phenomena of most interest are presented, and the nonlinear parameters used to quantify the strength of some nonlinearities in photonic materials are discussed.

### A.1.2 Nonlinear Polarization

In linear optics, when an electric field interacts with a material, an induced polarization arises, which depends linearly on the electric field intensity, and is given by:

$$\vec{P}(t) = \epsilon_0 \chi^{(1)} \vec{E}(t), \quad (5)$$

where  $\chi^{(1)}$  is known as the linear electric susceptibility and is related to the (linear) refractive index by  $n = \sqrt{1 + \chi}$ . As it was shown before, if the strength of the field is large enough, the nonlinearities of the interaction between the field and the material becomes important. The analytical relation between the electric field and the resulting polarization must be generalized, which is often done by expressing the polarization in terms of a power series of the field:

$$\vec{P}(t) = \epsilon_0 [\chi^{(1)} \vec{E}(t) + \chi^{(2)} \vec{E}^2(t) + \chi^{(3)} \vec{E}^3(t) + \dots] = \vec{P}^{(1)}(t) + \vec{P}^{(2)}(t) + \vec{P}^{(3)}(t) + \dots, \quad (6)$$

where  $\chi^{(2)}$ ,  $\chi^{(3)}$ ,  $\dots$  are called the second, third, ... order nonlinear optical susceptibilities. For the sake of simplicity, let's assume that the fields  $\vec{P}(t)$  and  $\vec{E}(t)$  are scalar quantities, which is a reductionist assumption as the nonlinear susceptibilities depend greatly on the polarization of light, but this holds for specific conditions (e.g., linearly polarized light, oriented along one of the material's principal axes) and helps to understand the phenomenon. The amount of significant terms required for the polarization vector expansion in power series depends on the strength of the field and the material itself; as they are only considered when they account for measurable phenomena. Nonlinear effects manifestations become significant when the strength of the field is comparable with the atomic electric fields, which have the order of magnitude of  $|\vec{E}_{at}| = e/4\pi\epsilon_0 a_0 = 5.14 \times 10^{11} \text{V/m}$ ,<sup>28</sup> where  $e$  is the charge of the electron,  $\epsilon_0$  is the free space permittivity, and  $a_0$  is the Bohr radius. So, the nonlinear phenomena associated to the second order susceptibility  $\chi^{(2)}$  will be relevant when

$$\chi^{(2)} \approx \frac{\chi^{(1)}}{E_{at}}. \quad (7)$$

The same holds for the third order susceptibility  $\chi^{(3)}$ :

$$\chi^{(3)} \approx \frac{\chi^{(1)}}{E_{at}^2}, \quad (8)$$

and so on. Since experimental observations are almost always direct measurements of irradiance, an approximated threshold for the intensity required to excite measurable nonlinearities may be formulated as:

$$I = \frac{1}{2} \epsilon_0 c |E_{at}|^2 = 3.5 \times 10^{16} \text{W/cm}^2.$$

Knowing this, the most commonly used materials in nonlinear photonics exhibit phenomena associated to the second-order susceptibility, and third-order susceptibility, as their corresponding nonlinear effects are usually more easily excited than nonlinearities of higher order. And  $P^{(2)}(t) = \epsilon_0 \chi^{(2)} E^2(t)$  is referred as the second-order nonlinear polarization, which gives account of the nonlinear phenomena associated to  $\chi^{(2)}$ , and  $P^{(3)}(t) = \epsilon_0 \chi^{(3)} E^3(t)$  is referred as the third-order nonlinear polarization, which gives account of the nonlinear phenomena associated to  $\chi^{(3)}$ . In order to detect significant nonlinear phenomena, an intense electromagnetic field must propagate through a material medium with relatively high nonlinear susceptibilities.

Then, to complete the presentation of the formalism, Eq. (6) is formulated as

$$P(t) = P^L(t) + P^{NL}(t), \quad (9)$$

where  $P^L(t)$  is the linear polarization in Eq. (5) and  $P^{NL}(t)$  contains all the nonlinear terms. Next, Eq. (9) can be replaced in the wave equation for propagation in a material, so that<sup>28</sup>

$$\nabla^2 E - \frac{1}{c_0^2} \frac{\partial^2 E}{\partial t^2} = \mu_0 \frac{\partial^2 P}{\partial t^2}; \quad P = P^L + P^{NL}, \quad (10)$$

where  $c_0$  is the speed of light in free space and  $\mu_0$  is the magnetic permeability in free space. Finally, Eq. (10) leads to the wave equation in nonlinear optical media

$$\nabla^2 E - \frac{n^2}{c_0^2} \frac{\partial^2 E}{\partial t^2} = \mu_0 \frac{\partial^2 P^{NL}}{\partial t^2}, \quad (11)$$

where  $P^{NL} = \epsilon_0 [\chi^{(2)} E^2(t) + \chi^{(3)} E^3(t)]$ , and only low-order nonlinear effects are considered. According to the form of  $P^{NL}$  different phenomena can occur, and by solving Eq. (11) it is found that new frequencies can be generated, and other effects as self-focusing and defocusing, self-phase modulation, nonlinear absorption, among others can be found as response to external very intense electric fields. In general,  $P^{NL}(t)$  is a vector and is called nonlinear polarization vector, but in this case the scalar approximation is held.

### A.1.3 Nonlinear Phenomena

The different nonlinear phenomena that are achievable for sufficiently intense electric field depends mainly on the material that is used as a media for the nonlinear propagation described in Eq. (11). This dependence is given by the nonlinear susceptibility  $\chi$ , which in general is a tensor with multiple entries. Due symmetries in the material crystalline structure some entries nullifies and therefore some phenomena are encouraged or not. For more information see references 28 and 29. The nonlinear phenomena can be classified into groups according to their relation with the nonlinear susceptibility. Thus, there are second-order nonlinear phenomena and third-order nonlinear phenomena. Usually materials that present important second-order susceptibility do not have an important third-order susceptibility, and vice versa.

Some second-order nonlinear phenomena are:

- **Second Harmonic Generation:** From light with frequency  $\omega$  is generated light with frequency  $2\omega$ .<sup>28</sup> It has applications in imaging,<sup>30</sup> spectroscopy and microscopy.<sup>31</sup>
- **Spontaneous Parametric Down-Conversion:** From light with frequency  $\omega$  is generated light with  $\omega/2$ .<sup>32</sup> It has applications in quantum optics in the generation of entangled photons.<sup>33</sup>
- **Three-Wave Mixing:** Or sum (difference) of frequencies. From two waves with frequency  $\omega_1$  and  $\omega_2$  a third wave of frequency  $\omega_3 = \omega_1 + \omega_2$  ( $\omega_3 = \omega_2 - \omega_1$ ) is generated.<sup>34</sup> It has applications in quantum entanglement,<sup>35</sup> and spectroscopy and microscopy.<sup>31</sup>

Some third-order nonlinear phenomena are:

- **Supercontinuum Generation:** From light of frequency  $\omega$  a continuum spectrum is achieved. If  $\omega$  is selected properly, white light can be generated from a laser.<sup>36,37</sup> It has applications in sensing<sup>38</sup> and microscopy.<sup>39</sup>
- **Four-Wave Mixing:** Or sum (difference) of frequencies. In general, from three waves with frequency  $\omega_1$ ,  $\omega_2$  and  $\omega_3$  a fourth wave of frequency  $\omega_4 = \omega_1 + \omega_2 + \omega_3$  is generated.<sup>29</sup> It has applications in optical parametric oscillators (OPO),<sup>40</sup> generation of entangled photons,<sup>41</sup> and Optical Phase Conjugation.<sup>42</sup>
- **Nonlinear Optical Kerr Effect:** The refractive index depends on the intensity of the laser, in this way the beam can be self-focused in the material or experience defocusing.<sup>28</sup>
- **Two-Photon Absorption:** Also known as nonlinear absorption, it is the simultaneous absorption of two photons by an atom, provoking its transition to an excited state with higher energy.<sup>28</sup>

This work is focused on the Two-Photon Absorption (TPA) and the Nonlinear Kerr Effect, since most of third-order nonlinear phenomena rely on those effects. To explain the change of the refractive index due a high intensity field, the nonlinear polarization for a beam interacting with a media with third-order susceptibility is described as:<sup>28</sup>

$$P^{NL}(\omega) = 3\epsilon_0\chi^{(3)}E(\omega)E(\omega)E(\omega). \quad (12)$$

As it has been shown, the polarization, and the electric field are time dependent. In nonlinear optics, it is pertinent to analyze the frequencies involved in the light-matter interaction. Therefore, it is useful to take the Fourier transform of the polarization vector to analyze the frequency dependency of the interaction. So, the total polarization will be given by the Fourier transform of Eq. (9):

$$\begin{aligned}
 P &= P^L(\omega) + P^{NL}(\omega) = \epsilon_0\chi^{(1)}E(\omega) + 3\epsilon_0\chi^{(3)}E(\omega)E(\omega)E(\omega) \\
 &= \epsilon_0 \underbrace{[\chi^{(1)} + 3\chi^{(3)}|E(\omega)|^2]}_{\chi_{eff}} E(\omega) \\
 &= \epsilon_0\chi_{eff}E(\omega),
 \end{aligned} \tag{13}$$

where  $\chi_{eff} = \chi^{(1)} + 3\chi^{(3)}|E(\omega)|^2$  is the effective permittivity. This is the permittivity of the material taking into account the third-order susceptibility. Under the linear approximation, the refractive index can be written in terms of the permittivity<sup>43</sup> as

$$n^2 = 1 + \chi; \tag{14}$$

so, the refractive index is generalized for nonlinear studies by taking into account the third order-susceptibility, which gives rise to the expression

$$n^2 = 1 + \chi_{eff} = 1 + \chi^{(1)} + 3\chi^{(3)}|E(\omega)|^2 \longrightarrow n = \sqrt{1 + \chi^{(1)} + 3\chi^{(3)}|E(\omega)|^2}. \tag{15}$$

Using Eq. (14), the linear refractive index can be defined as  $n_0^2 = 1 + \chi^{(1)}$ , and Eq. (15) takes the form

$$n = \sqrt{n_0^2 \left( 1 + \frac{3\chi^{(3)}|E(\omega)|^2}{n_0^2} \right)}. \tag{16}$$

As the quotient  $\chi^{(3)}|E(\omega)|^2/n_0^2$  is a very small number, the binomial approximation  $(1 + x)^n \approx 1 + nx$  for  $x \ll 1$  may be applied. So, the refractive index definition is written as

$$n \approx n_0 + \frac{3}{2} \frac{\chi^{(3)}}{n_0} |E(\omega)|^2. \tag{17}$$

The electric field can be written as:

$$E(\omega) = \frac{1}{2} \tilde{E}(\omega) e^{-i\omega t}; \tag{18}$$

therefore, the irradiance:

$$I = \frac{1}{2} n_0 \epsilon_0 c |E(\omega)|^2. \tag{19}$$

Replacing Eq. (19) into Eq. (17), the refractive index becomes dependent from irradiance by taking into account the third-order susceptibility. This is:

$$n = n_0 + \frac{3}{2} \frac{\chi^{(3)}}{n_0^2 \epsilon_0 c} I. \tag{20}$$

But the refractive index has both real and imaginary parts:<sup>43</sup>

$$n = Re\{n\} + i Im\{n\} = Re\{n\} - i \frac{\alpha}{2k_0} \quad (21)$$

where  $Re\{n\}$  is commonly known as refractive index and  $\alpha$  is related to the losses by absorption, called the absorption coefficient. So, Eq. (20) yields:

$$Re\{n\} - i \frac{\alpha}{2k_0} = Re\{n_0\} - i \frac{\alpha_0}{2k_0} + \frac{3\chi^{(3)}}{n_0^2\epsilon_0 c} I, \quad (22)$$

where the third-order susceptibility is in general a complex value quantity, and the complex-valued  $n_0$  was decomposed into its real and imaginary parts in a similar way as it was done for  $n$  in Eq. (21). So, equating the real and imaginary parts of Eq. (22), it is obtained for the refractive index and the absorption coefficient:

$$Re\{n\} = Re\{n_0\} + \frac{3}{n_0^2\epsilon_0 c} Re\{\chi^{(3)}\} I = Re\{n_0\} + n_2 I, \quad (23a)$$

$$\alpha = \alpha_0 - \frac{6\omega_0}{n_0^2\epsilon_0 c^2} Im\{\chi^{(3)}\} I = \alpha_0 + \beta_{TPA} I, \quad (23b)$$

where

$$n_2 = \frac{3}{n_0^2\epsilon_0 c} Re\{\chi^{(3)}\}, \quad (24a)$$

is called the nonlinear refractive index, and

$$\beta_{TPA} = -\frac{6\omega_0}{n_0^2\epsilon_0 c^2} Im\{\chi^{(3)}\}, \quad (24b)$$

is called the two-photon absorption coefficient. Now it become evident, by inspecting Eqs. (23), that in general the refractive index is irradiance-dependent, but this is only relevant when the medium of propagation has significant third-order susceptibility.

## A.2 THEORETICAL FRAMEWORK

One of the most useful and pervasive techniques for the characterization of nonlinear optical properties is known as Z-scan. It was first introduced by Sheik-Bahae, *et. al.* in 1989<sup>44</sup> as a simple but promising methodology for the sensitive quantification of the nonlinear response of new photonic materials. It can be used for measuring the two-photon absorption coefficient  $\beta_{TPA}$  and the nonlinear refractive index  $n_2$  of the material under study. And unlike other techniques, it allows the direct determination of the sign of the nonlinear index.

In general, the basic implementation of the Z-scan technique comprises a converging lens, a photodetector, and a blocking element (e.g., a diaphragm or a mask) that only allows light propagation within a small aperture. All elements form an axisymmetric optical system, with a single propagation axis, as illustrated in Fig. 3. Intense laser light enters the system through the lens, and is detected after the focal plane. The blocking element with the small aperture is placed right before the detector, in such a way that it can be removed or its aperture can be widen. This will enable to switch between two measuring modalities: closed-aperture detection and open-aperture detection. The sample is placed between the lens and the aperture.<sup>21</sup>

The convergence and divergence effects that the lens induce on the propagation of the beam, introduce a direct connection between spatial coordinates and irradiance levels; therefore, if the focused laser beam is scanned along the  $z$ -axis with the sample, an irradiance sweep is performed, and the irradiance-dependent attenuation and refraction are probed. As the sampled gets exposed to higher irradiance levels, it simultaneously absorbs a greater fraction of the incident power and exhibits a more notorious lensing effect. The first occurs due to the increase of two-photon absorption losses; as this light-matter interaction event becomes more likely. The second

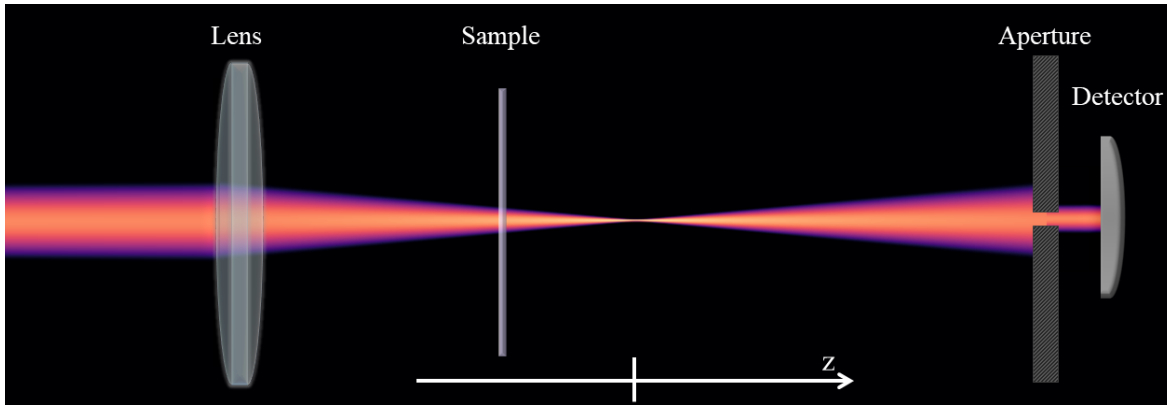


Figure 3. Schematic diagram of the optical system used for the Z-scan technique.

is a consequence of the radial distribution of the irradiance-dependent refractive index variation, which inherits the functional form of the transverse irradiance profile; the resulting radially-varying phase-shift has a focusing or defocusing effect, that gets stronger with the exposition to greater irradiance levels.

To study these two phenomena separately, the aperture is employed. The measurement of the open-aperture detection is not influenced by the refractive effects, if the photodetector sensitive area is large enough as for detecting most of the optical power that gets to the aperture and detection planes under any configuration of the optical system. Thereby, the open-aperture measurements are only affected by the nonlinear absorption processes. In contrast, the closed-aperture measurements are affected by the nonlinear refraction, since the power that passes through the fixed aperture depends on how expanded or collimated is the beam at the aperture plane. If the nonlinear refractive index of the sample is positive, the irradiance-dependent lensing effect is convergent, and the beam at the aperture plane gets expanded when the sample is placed before the focus (closer to the lens), and collimated when the sample is placed after the focus (closer to the photodetector). If the nonlinear refractive index of the sample is negative, the contrary happens because irradiance-dependent lensing effect is divergent. Then, the closed-aperture detection holds the information about the sign of the  $n_2$  refractive index as well.

Closed-aperture measurements are likewise affected by nonlinear optical losses. So, in order to study the nonlinear refractive effects independently, it is necessary to subtract the nonlinear attenuation effects from the closed-aperture detection. This is achieved by normalizing the closed-aperture signal, with respect to the open-aperture signal.

Then, the Z-scan experimental methodology can be summarized as follows. Keeping the aperture open, the sample is first moved along the laser light propagation axis, passing through the focal plane. The optical power after the aperture plane is monitored during the scan with the photodetector. Next, the scan is performed under the same conditions, but keeping the aperture closed. As explained, the information obtained from these two scans along the z-axis (hence the name of the technique) are sufficient for the determination of the third-order nonlinear parameters  $\beta_{TPA}$  and  $n_2$  of the sample. Detailed experimental steps are explained in section A.3.

### A.2.1 Modeling approach and slowly varying envelope approximation

To describe the optical fields involved in a Z-scan system, a wave optics model is employed. In the following derivations, light is assumed to preserve its linear polarization state; so anisotropic effects within the sample will not be considered. And the external medium will be assumed to be air. The laser light could either carry a constant power over time, or be pulsed to attain greater instantaneous power levels. And in this work, optical nonlinearities are assumed to appear instantaneously, right after the material is exposed to the intense optical excitation. This approximation is certainly accurate in the cases in which pulsed light is used, with very short pulse duration with respect to the time response of material's thermal nonlinear optical effects. Before the sample, the focused laser light is modeled as a Gaussian beam, following the analytical formulation given by the Eq. (25),<sup>21,43</sup>

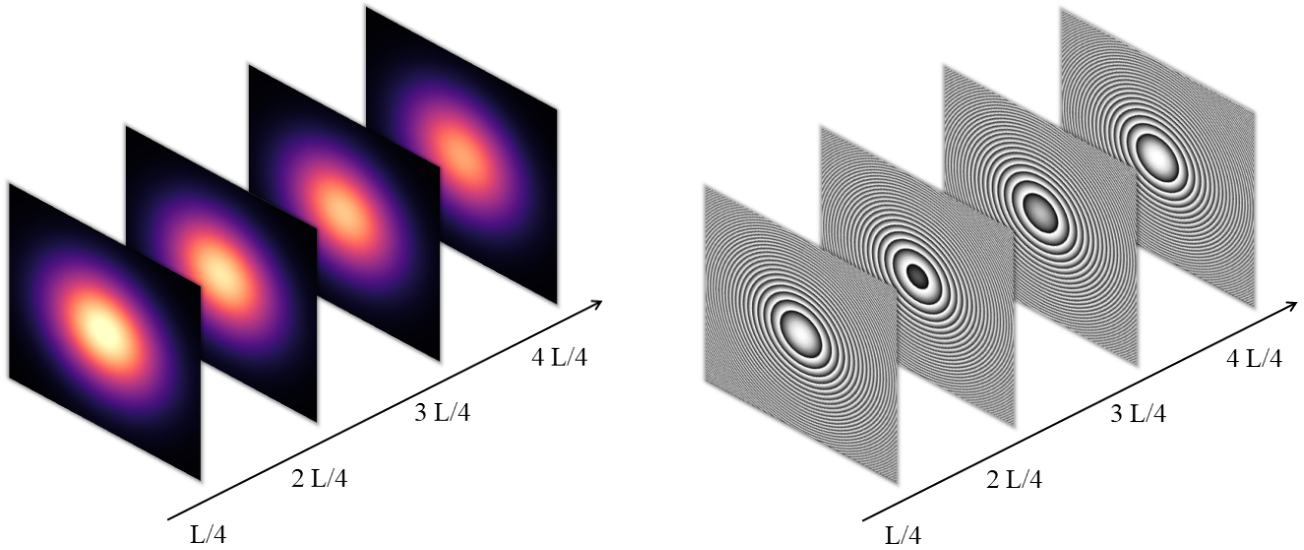
$$E(z, r, t) = E_0(t) \frac{w_0}{w(z)} \exp \left[ -\frac{r^2}{w^2(z)} - \frac{ik_0 r^2}{2R(z)} \right] \exp[-i\varphi(z, t)], \quad (25)$$

where  $z$  and  $r$  are axial and radial coordinates,  $k_0$  is the vacuum wavenumber of the beam,  $E_0(t)$  is the temporally-modulated electric field's complex amplitude at focus,  $w_0$  is the radius of the beam at focus,  $\exp[-i\varphi(z, t)]$  is a conventional phase propagation term, and

$$w^2(z) = w_0^2 \left( 1 + \frac{z^2}{z_0^2} \right), \quad R(z) = z \left( 1 + \frac{z_0^2}{z^2} \right), \quad z_0 = \frac{k_0 w_0^2}{2}. \quad (26)$$

After the sample, the propagation and power calculations must take into account the radially-varying phase-shift and power attenuation introduced by the sample; which produce deviations from the Gaussian formulation. Fourier optics propagation methods are very useful for these far-field calculations, especially for numerical implementations.

The propagation of the optical field within the sample is, in general, influenced by the linear and nonlinear absorption, linear and nonlinear refraction, and natural diffraction processes. If the sample is thin (i.e., with thickness  $L$  shorter than beam's Rayleigh length  $z_0$ <sup>21</sup>), the diffraction and refraction phenomena may be neglected for the study of the evolution of the beam within the sample. This approach is known as slowly varying envelope approximation (SVEA), and entails that the beam transverse profile preserves its size (see Fig. 4). Thereby, the nonlinear phase-shift that results from the propagation throughout the nonlinear medium is only taken into account for the far field propagation, between the sample and the detector. It is important to notice that this approximation does not imply that the irradiance distribution of the beam is not tracked within the sample: it gets attenuated as consequence of absorption processes, and its decay rate distribution is determinant in the description of the considered nonlinear effects.



(a) The irradiance profile of the beam within the sample is assumed to preserve its size. Under the SVEA, the beam behaves as a plane wave with a radially-modulated irradiance distribution.

(b) Under the SVEA, the phase evolution of the beam does not influence the propagation analysis within the sample. However, the accumulated phase-shift distribution comes into effect in the subsequent far-field propagation study.

Figure 4. Slowly varying envelope approximation, for thin media, facilitates the analytical description of the nonlinear phenomena under study. It assumes that the beam is neither converging, nor diverging within the sample.

In this way, the irradiance profile evolution within the sample is described by the Eq. (27), and the accumulated phase-shift can be calculated using Eq. (28):<sup>21</sup>

$$\frac{\partial I}{\partial \ell} = -\alpha I; \quad (27)$$

$$\frac{\partial \Delta\phi}{\partial \ell} = \Delta n k_0. \quad (28)$$

To avoid confusion,  $\ell$  is used to denote the coordinate along the propagation axis for calculations within the sample, and  $z$  is used to denote position along the propagation axis at which the sample is placed (coordinate of the sample's input facet).  $\ell = 0$  at sample's input facet, and  $z = 0$  at beam's focus.

### A.2.2 Nonlinear phase-shift: for negligible nonlinear absorption

In general, the attenuation coefficient  $\alpha$  in Eq. (27) can have an irradiance-independent part and an irradiance-dependent one (23b). If the nonlinear absorption processes have a very low probability to occur, the power attenuation in the material is essentially linear, and  $\alpha \approx \alpha_0$ . In this case, the solution to Eq. (27) becomes

$$I = I(\ell = 0) e^{-\alpha_0 \ell}. \quad (29)$$

This expression for the irradiance evolution allows to calculate the accumulated irradiance-dependent phase-shift variation. Thus, using Eqs. (23a), (28), and (29), for a sample with thickness  $L$ , it is found that

$$\Delta\phi = \int_0^L \Delta n(I) k_0 d\ell = k_0 \int_0^L n_2 I d\ell = k_0 n_2 I(\ell = 0) \int_0^L e^{-\alpha_0 \ell} d\ell; \quad (30a)$$

$$\Delta\phi = k_0 n_2 I(\ell = 0) \frac{1 - e^{-\alpha_0 L}}{\alpha_0}. \quad (30b)$$

It is possible to notice that the last factor in Eq. (30b) has length dimension, and it can be regarded as an effective length for the nonlinear phenomenon. This means that the nonlinear phase-shift variation that is accumulated through the propagation in the lossy medium with thickness  $L$ , could be equally calculated as the one that would be accumulated after the constant-irradiance propagation through a non-lossy medium with thickness  $L_{eff}$ ; being

$$L_{eff} = \frac{1 - e^{-\alpha_0 L}}{\alpha_0}. \quad (31)$$

Then, the nonlinear phase-shift is calculated for media without nonlinear absorption as follows<sup>21</sup>

$$\Delta\phi = k_0 n_2 L_{eff} I(\ell = 0) = k_0 n_2 L_{eff} I_0(t) \frac{1}{1 + \frac{z^2}{z_0^2}} \exp \left[ -\frac{2r^2}{w^2(z)} \right], \quad (32)$$

where  $I(\ell = 0) = I(z, r, t)$  is the irradiance distribution of the Gaussian beam, derived from the Eq. (25); with  $r$  and  $z$  evaluated at sample's input face plane, and  $I_0(t)$  evaluated at beam's focus.

### A.2.3 Nonlinear phase-shift: considering nonlinear absorption

If the nonlinear absorption is appreciable, the irradiance profile evolution is described by the differential equation

$$\frac{\partial I}{\partial \ell} = -\alpha_0 I - \beta_{TPA} I^2; \quad (33)$$

whose solution, by separation of variables, requires the calculation of the antiderivative

$$\ell + K^{(A)} = \int \frac{1}{-\alpha_0 I - \beta_{TPA} I^2} dI. \quad (34)$$

It may be obtained by partial fractions decomposition, as follows:

$$\int \frac{1}{-\alpha_0 I - \beta_{TPA} I^2} dI = \int \frac{\beta_{TPA}}{\alpha_0(\alpha_0 + \beta_{TPA} I)} dI - \int \frac{1}{\alpha_0 I} dI = \frac{1}{\alpha_0} \ln[\alpha_0 + \beta_{TPA} I] - \frac{1}{\alpha_0} \ln[I] + K^{(B)}; \quad (35a)$$

$$\therefore \ell = \frac{1}{\alpha_0} \ln \left[ \frac{\alpha_0 + \beta_{TPA} I}{I} \right] + K^{(C)}. \quad (35b)$$

Thus, an expression for the irradiance dependence on  $\ell$  is derived:

$$K^{(D)} e^{-\alpha_0 \ell} = \frac{I}{\alpha_0 + \beta_{TPA} I} \longleftrightarrow I(\ell) = \frac{K^{(D)} \alpha_0 e^{-\alpha_0 \ell}}{1 - K^{(D)} \beta_{TPA} e^{-\alpha_0 \ell}}. \quad (36)$$

If the irradiance profile at the input facet is known, the parameter  $K^{(D)}$  is calculated as

$$K^{(D)} = \frac{I(\ell = 0)}{\alpha_0 + \beta_{TPA} I(\ell = 0)}, \quad (37)$$

and Eq. (36) takes the form<sup>21</sup>

$$I(\ell) = \frac{e^{-\alpha_0 \ell}}{1 + \frac{\beta_{TPA}}{\alpha_0} (1 - e^{-\alpha_0 \ell}) I(\ell = 0)} I(\ell = 0). \quad (38)$$

All parameters  $K^{(\cdot)}$  are arbitrary constants.

Last expression describes the evolution of the irradiance, taking into account the nonlinear absorption effects, and allows to calculate the corresponding irradiance-dependent phase-shift variation. Using Eqs. (23a), (28) and (38) it is found that

$$\Delta\phi = \int_0^L \Delta n(I) k_0 d\ell = k_0 n_2 \int_0^L \frac{e^{-\alpha_0 \ell}}{1 + \frac{\beta_{TPA}}{\alpha_0} (1 - e^{-\alpha_0 \ell}) I(\ell = 0)} I(\ell = 0) d\ell; \quad (39)$$

if the denominator's expression is expanded and the substitution  $u = \frac{\beta_{TPA} I(\ell=0)}{\alpha_0} e^{-\alpha_0 \ell}$  is introduced, one obtains

$$\Delta\phi = \frac{k_0 n_2}{\beta_{TPA}} \int_{u(\ell=0)}^{u(\ell=L)} \frac{1}{-\left(1 + \frac{\beta_{TPA} I(\ell=0)}{\alpha_0}\right) + u} du; \quad (40)$$

which can be easily solved by introducing the second substitution  $v = -\left(1 + \frac{\beta_{TPA} I(\ell=0)}{\alpha_0}\right) + u$ , as it yields

$$\Delta\phi = \frac{k_0 n_2}{\beta_{TPA}} \int_{v(u(\ell=0))}^{v(u(\ell=L))} \frac{1}{v} dv = \frac{k_0 n_2}{\beta_{TPA}} \ln|v| \Big|_{v(u(\ell=0))}^{v(u(\ell=L))}. \quad (41)$$

By replacing  $u$  and  $v$ , the following expression results for the nonlinear phase-shift variation profile:<sup>21</sup>

$$\Delta\phi = \frac{k_0 n_2}{\beta_{TPA}} \ln \left| \frac{\beta_{TPA} I(\ell=0)}{\alpha_0} e^{-\alpha_0 \ell} - \frac{\beta_{TPA} I(\ell=0)}{\alpha_0} - 1 \right| \Bigg|_{\ell=0}^{\ell=L}; \quad (42a)$$

$$\therefore \Delta\phi = \frac{k_0 n_2}{\beta_{TPA}} \ln \left| 1 + \frac{\beta_{TPA} I(\ell=0)}{\alpha_0} (1 - e^{-\alpha_0 L}) \right| = \frac{k_0 n_2}{\beta_{TPA}} \ln [1 + \beta_{TPA} L_{eff} I(\ell=0)]. \quad (42b)$$

#### A.2.4 Formulation in terms of measurable quantities

Within the wave optics approach, beam's irradiance and phase profiles are the physical entities directly affected by the nonlinearities of the material. However, to connect this theoretical framework with the observations carried out in the laboratory, it is necessary to derive a description of the nonlinearities manifestation in terms of average optical power measurements.

As it was explained at the start of this section, the nonlinear absorption may be directly associated with the deviations from the linear regime that appear in open-aperture measurements. Therefore, it is convenient to find the analytical expression for the optical power that would be measured after the sample, given the irradiance profile previously obtained (Eq. (38)). For this aim, the irradiance profile is integrated across the sample's output facet plane. This power value is expected to be same for any detection plane after that sample, since the propagation in air is assumed to be lossless. Considering that  $I(\ell=0) = I(z, r, t)$  is the irradiance profile of the Gaussian beam, with  $r$  and  $z$  evaluated at sample's input facet plane, and  $I_0(t)$  evaluated at beam's focus, the integration process is summarized as follows:

$$P(\ell=L) = \iint_S I(\ell=L) dA = \iint_S \frac{e^{-\alpha_0 L} I(\ell=0)}{1 + \beta_{TPA} L_{eff} I(\ell=0)} dA; \quad (43a)$$

$$P(\ell=L) = \iint_S \frac{e^{-\alpha_0 L} I_0(t) \frac{1}{1+z^2/z_0^2} e^{-2r^2/w^2(z)}}{1 + \beta_{TPA} L_{eff} I_0(t) \frac{1}{1+z^2/z_0^2} e^{-2r^2/w^2(z)}} dA = \iint_S \frac{e^{-\alpha_0 L} e^{-2r^2/w^2(z)}}{\frac{1+z^2/z_0^2}{I_0(t)} + \beta_{TPA} L_{eff} e^{-2r^2/w^2(z)}} dA; \quad (43b)$$

$$P(\ell=L) = e^{-\alpha_0 L} \int_0^{2\pi} \int_0^\infty \frac{e^{-2r^2/w^2(z)}}{\Lambda + \Omega e^{-2r^2/w^2(z)}} r dr d\theta = 2\pi e^{-\alpha_0 L} \int_0^\infty \frac{e^{-2r^2/w^2(z)}}{\Lambda + \Omega e^{-2r^2/w^2(z)}} r dr; \quad (43c)$$

with  $\Lambda = \frac{1+z^2/z_0^2}{I_0(t)}$  and  $\Omega = \beta_{TPA} L_{eff}$  to ease the notation. Then, with  $u = -2r^2/w^2(z)$  and  $v = \Lambda + \Omega e^u$ , the integration by substitution yields

$$P(\ell=L) = -\frac{\pi w^2(z) e^{-\alpha_0 L}}{2} \int_{u(r=0)}^{u(r \rightarrow \infty)} \frac{e^u}{\Lambda + \Omega e^u} du = -\frac{\pi w^2(z) e^{-\alpha_0 L}}{2\Omega} \int_{v(u(r=0))}^{v(u(r \rightarrow \infty))} \frac{1}{v} dv; \quad (43d)$$

$$P(\ell=L) = -\frac{\pi w^2(z) e^{-\alpha_0 L}}{2\Omega} \ln|v| \Big|_{v(u(r=0))}^{v(u(r \rightarrow \infty))} = -\frac{\pi w^2(z) e^{-\alpha_0 L}}{2\Omega} \ln \left| \Lambda + \Omega e^{-2r^2/w^2(z)} \right| \Big|_{r=0}^{r \rightarrow \infty}; \quad (43e)$$

$$\therefore P(\ell=L) = \frac{\pi w^2(z) e^{-\alpha_0 L}}{2\beta_{TPA} L_{eff}} \ln \left[ 1 + \frac{\beta_{TPA} L_{eff} I_0(t)}{1 + z^2/z_0^2} \right]. \quad (43f)$$

To express Eq. (43f) in terms of measurable values of input power, a similar integration procedure is carried out for the input irradiance profile; i.e., Gaussian beam's irradiance  $I(\ell=0) = I(z, r, t)$ . In this case, the substitution  $u = -2r^2/w^2(z)$  and the definition of  $w^2(z)$  from Eqs. (26) are employed.

$$P(\ell=0) = \iint_S I(\ell=0) dA = \int_0^{2\pi} \int_0^\infty I_0(t) \frac{1}{1 + z^2/z_0^2} e^{-2r^2/w^2(z)} r dr d\theta; \quad (44a)$$

$$P(\ell=0) = 2\pi \frac{I_0(t)}{1 + z^2/z_0^2} \int_0^\infty e^{-2r^2/w^2(z)} r dr = -\frac{\pi w_0^2}{2} I_0(t) \int_0^{-\infty} e^u du = \frac{\pi w_0^2}{2} I_0(t); \quad (44b)$$

$$\therefore I_0(t) = \frac{2}{\pi w_0^2} P(\ell = 0). \quad (44c)$$

Finally, if the used laser source is pulsed, it is important to take into consideration that the measurements made by a photodetector correspond to average optical power, and previously derived expression are valid for instantaneous power values. Thus, a relation must be established between the instantaneous peak power and the detected average power. To simplify the analytical model, the temporal envelope of the pulse is assumed to have a rectangular shape. This means that for a laser source with pulse duration  $\tau$  and repetition rate  $f_{rep} = 1/T$ , the instantaneous optical power is given by

$$P(\ell) = \begin{cases} \bar{P}(\ell)/(\tau f_{rep}), & \text{if } 0 \leq t < \tau; \\ 0, & \text{if } \tau \leq t < T; \end{cases} \quad (45a)$$

since the average power  $\bar{P}$  and peak power  $\hat{P}$  are related by their dependence with the energy of the pulse  $\mathcal{E}_{pulse}$ :

$$\bar{P} = \frac{\mathcal{E}_{pulse}}{T} = \frac{\hat{P} \tau}{T} = \hat{P} \tau f_{rep} \leftrightarrow \hat{P} = \frac{\bar{P}}{\tau f_{rep}}. \quad (45b)$$

Then, using Eqs. (26), (44c) and (45b), the outgoing optical power expression from Eq. (43f) can be written in terms of average power values, as follows:<sup>21</sup>

$$\bar{P}_{out} = \tau f_{rep} e^{-\alpha_0 L} \frac{\pi w_0^2 \left(1 + \frac{z^2}{z_0^2}\right)}{2\beta_{TPA} L_{eff}} \ln \left[ 1 + \frac{2\beta_{TPA} L_{eff}}{\pi w_0^2 \left(1 + \frac{z^2}{z_0^2}\right) \tau f_{rep}} \frac{\bar{P}_{in}}{\tau f_{rep}} \right]. \quad (46)$$

Eq. (46) constitutes a ready-to-use expression to analyze experimental open-aperture input/output power measurements.

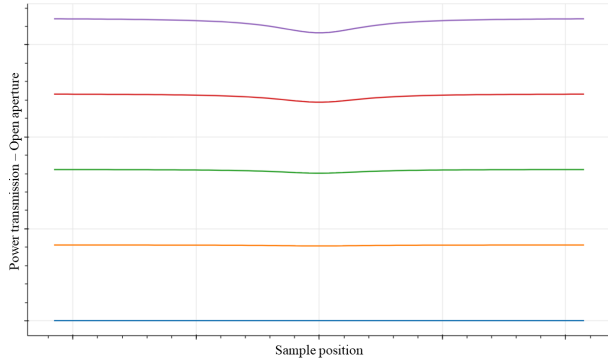
To obtain the corresponding theoretical description for the closed-aperture power measurements, it is necessary to calculate the electric field profile at the aperture plane, taking into account the details of the propagation between the sample and the aperture. In this work, this step is carried out by numerical means, using Fourier optics propagation methods. Thereby, the analytical formulation that is needed for this numerical implementation is the one describing the electric field's complex amplitude profile at the sample's output facet plane. The norm of this complex amplitude can be obtained from the expression for the output irradiance profile (Eq. (38)), which multiplied by the phase factor that accounts for the nonlinear phase-shift variation (Eq. (42b)) yields<sup>21</sup>

$$E(\ell = L) = \frac{e^{-\frac{\alpha_0 L}{2}} E(\ell = 0)}{[1 + \beta_{TPA} L_{eff} I(\ell = 0)]^{\frac{1}{2}}} e^{i\Delta\phi} = \frac{e^{-\frac{\alpha_0 L}{2}} E(\ell = 0)}{[1 + \beta_{TPA} L_{eff} I(\ell = 0)]^{\frac{1}{2}}} e^{i \frac{k_0 n_2}{\beta_{TPA}} \ln[1 + \beta_{TPA} L_{eff} I(\ell = 0)]}; \quad (47a)$$

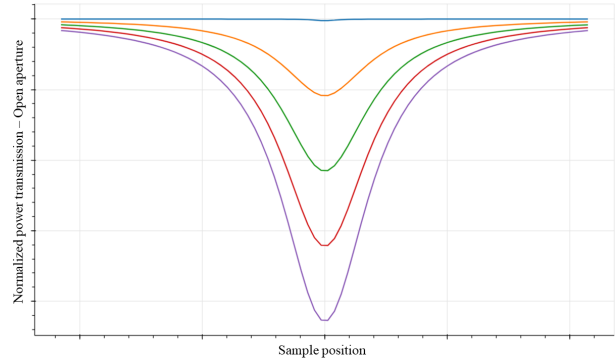
$$\therefore E(\ell = L) = e^{-\frac{\alpha_0 L}{2}} E(\ell = 0) [1 + \beta_{TPA} L_{eff} I(\ell = 0)]^{i \frac{k_0 n_2}{\beta_{TPA}} - \frac{1}{2}}. \quad (47b)$$

In the previous expression,  $E(\ell = 0)$  and  $I(\ell = 0)$  correspond to the Gaussian beam's electric field and irradiance profiles,  $E(z, r, t)$  and  $I(z, r, t)$ , evaluated at sample's input facet plane; which may be obtained from Eq. (25).

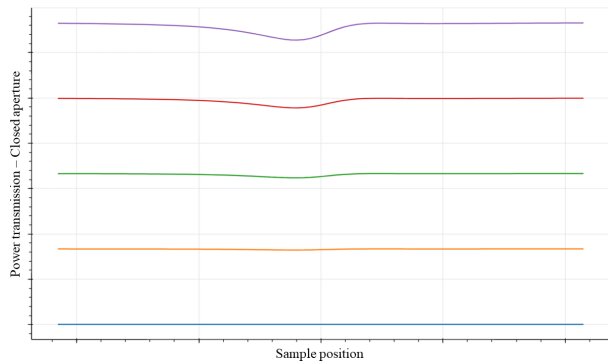
To illustrate the functional form of the output signals predicted by the model, transmission curves for open-aperture and closed-aperture setup configurations are presented in Fig. 5. Different input power levels were considered, to illustrate the typical evolution of the nonlinear material's response as incident power increases. Fig. 5(a) shows the optical power transmission predicted by Eq. (46) for open-aperture measurements; and Fig. 5(b) presents the scaled version of these open-aperture curves, taking as power reference the (maximum) transmission obtained in the linear range of the Z-scan. Likewise, Fig. 5(c) shows the power transmission for the closed-aperture case, obtained by numerically calculating the propagation of the electric field profile described by Eq. (47b). The numerical implementation used for this calculation is detailed in section B. Fig. 5(d) presents the normalized version of these closed-aperture curves, after the nonlinear absorption effects subtraction, and taking as power reference the transmission obtained in the linear range of the closed-aperture Z-scan.



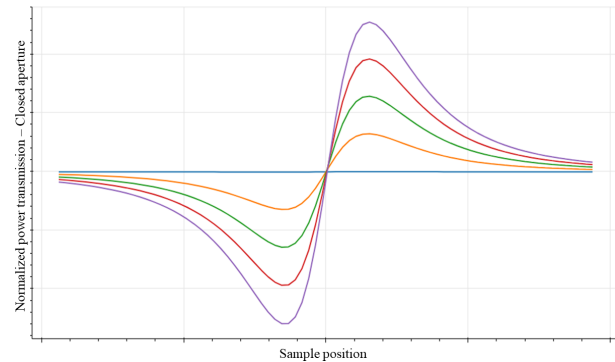
(a) Typical open-aperture power transmission (in arbitrary power units).



(b) Typical scaled open-aperture power transmission (adimensional).



(c) Typical closed-aperture power transmission (in arbitrary power units).



(d) Typical normalized closed-aperture power transmission (adimensional).

Figure 5. Typical power transmission curves theoretically predicted by the previously derived model, for different input power levels. Curves of the same color correspond to the same input power. Sample position is measured in arbitrary length units.

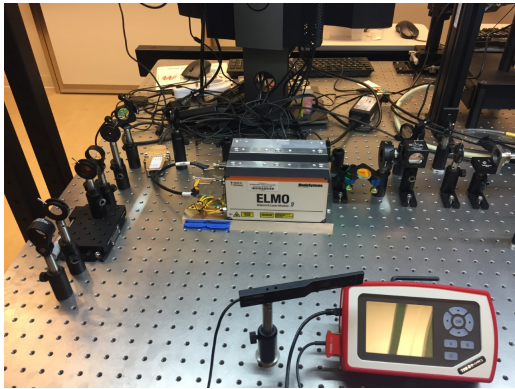
### A.3 EXPERIMENTAL SETUP AND PROCEDURES

#### A.3.1 Experimental Setup

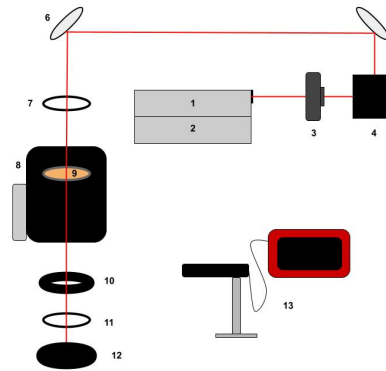
Fig. 6(a) and diagram 6(b) illustrate the optical bench setup used in the Z-Scan experiment in free-space. Table 2 details the optical elements that the experimental setup comprises.

Table 2. Experimental Equipment

1 Menlo Systems Amplifier ELMA	2 Menlo Systems Femtosecond Laser ELMO
3 Rotating Half-Wave Plate	4 Polarizing Beam splitter
5 Post-Mounted Optical Mirror	6 Post-Mounted Optical Mirror
7 Post-Mounted Lens	8 Thorlabs One-Dimensional Translation Stage
9 Post-Mounted Sample	10 Post-Mounted Adjustable Iris
11 Post-Mounted Lens	12 Post-Mounted Beam Blocker
13 Thorlabs Power Meter	



(a) Experimental setup image.



(b) Experimental setup diagram.

Figure 6.

### A.3.2 Sample Preparation and Mounting

Before beginning the Z-Scan process one must take proper care while mounting the sample. Be sure to wear gloves to avoid damaging the sample. One can mount a sample onto an iris that is secured in the open position with double sided tape, taking care not to obscure the beam path with the tape.

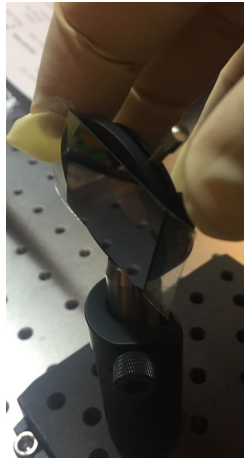


Figure 7. Mounting the sample.

The sample can then be mounted onto the translation stage by carefully screwing the iris mount into the post holder that is mounted onto the translation stage. Ensure the sample is perpendicular to the beam path in the experimental setup.

### A.3.3 Laser Activation

With the sample mounted, it is time to turn on the laser. Begin by turning on the computer connected to the laser at the optical bench. Locate the 'ELMO Software'.

Once the 'Elmo software' is running, one will see the startup menu in Fig. 9(a). Select the 'Subsystems' tab as seen in Fig. 9(b) and press the 'Elmo is On' and 'Elma is On' buttons. Now you will see the text to the right of these buttons turns from orange to green and the text in the buttons changes as seen in Fig. 9(c).

Double check the Elmo laser system to see the lights have turned green. Finally pull up the laser safety shutter to allow the laser pulses to exit the laser system and follow the beam path. Make sure to check the beam path with a photo-phosphorescent viewing card to ensure the beam is aligned properly.

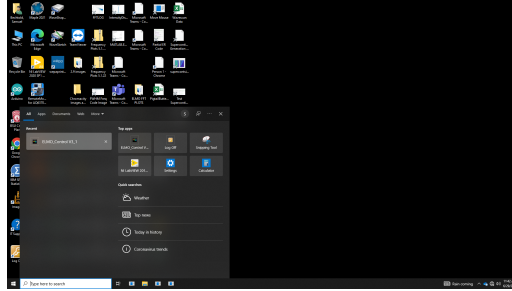


Figure 8. Elmo Control V3 Software

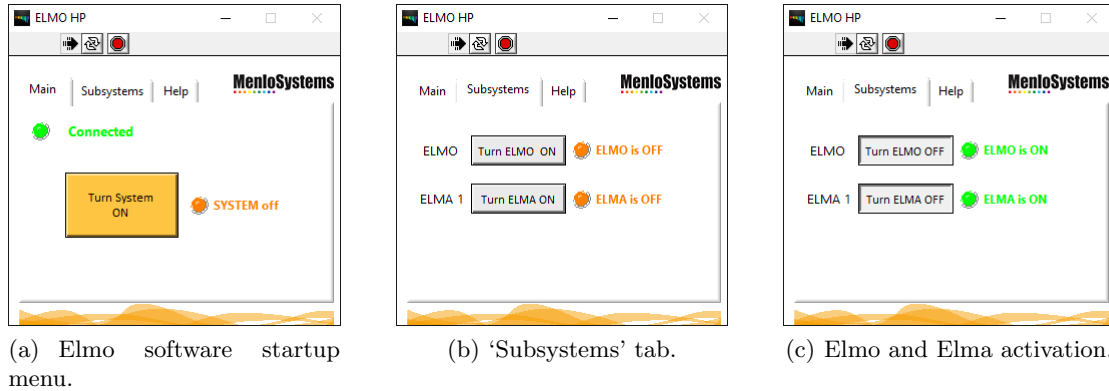


Figure 9.

### A.3.4 Pre-Measurement Procedures

Set the aperture size for the adjustable iris to ensure that for all of our scans the aperture size is the same. Begin by taking the power measurement with the Thorlabs power-meter immediately before the lens that lies before the sample stage. This power reading should be the same for all the aperture size calibrations, in our lab we use 100 mW.

To adjust the power of the laser, turn the gear of the Half-Wave Plate's mount until the power-meter reads the desired value. Finally, move the power meter immediately behind our adjustable aperture and measure the power as we adjust the aperture size to a predetermined amplitude, in our lab we use 18 mW. This aperture size calibration is needed if a post-mounted iris is used as blocking element in closed-aperture measurements. This process can be bypassed if another element was used, with a fixed aperture size, such as a precision pinhole.

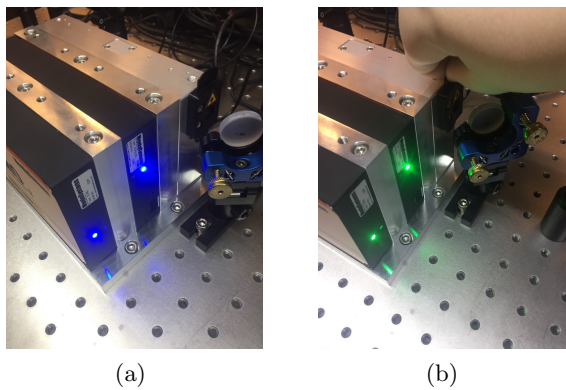


Figure 10. (a) Menlo Systems Elmo Femtosecond Laser with blue lights indicating that the laser is turned off. (b) Elmo Femtosecond Laser with green lights indicating that the laser is turned on.

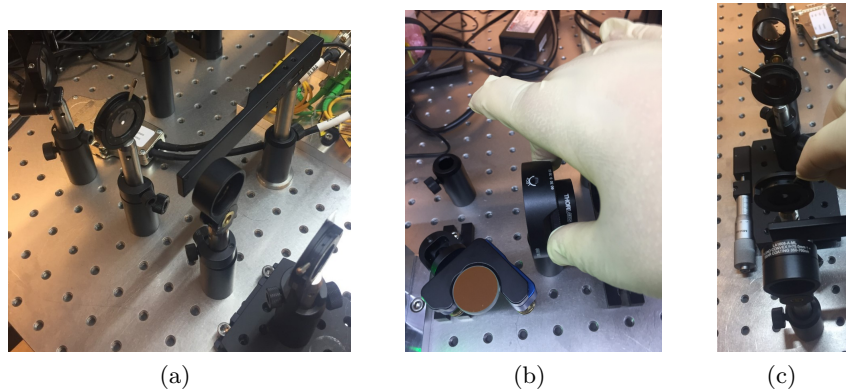


Figure 11. (a) Measure power before pre-sample lens. (b) Adjusting the laser power with the half-wave plate mount. (c) Adjusting the iris aperture size.

### A.3.5 Z-Scan Procedures

The Z-Scan consists of two types of scans, to be performed sequentially. The closed-aperture (CA) and open-aperture (OA) scans, as mentioned in previous section. To fully characterize the sample material, one must perform several Z-scans, making up a power sweep. A sweep is a series of scans over a range of incident power levels. For efficiency one should begin each set of scans by setting the aperture size as described in the Pre-Measurement Procedures section. After the aperture size is set, locate the power-meter immediately before the sample to adjust the incident power level.



Figure 12. Setting the laser power before the sample.

Remember that the power can be adjusted by turning the mount of the half-wave plate as seen in Fig. 11(a). Once at the desired power level, it is time to set up the closed-aperture Z-Scan (followed by an open-aperture Z-Scan). Make sure to move the power-meter directly behind the iris aperture and turn off any lights on the optical bench. Connect the power-meter to a laptop and turn on the Thorlabs Optical Power Monitor software.

Once connected to the software window, find the settings menu on the default display page and find the beam parameters section. Under 'profile', make sure that 'Gaussian' is selected on the drop down menu. Select the 'Monitoring' tab on the top left menu bar. Upon selection a 'Table Configuration' window will pop up, prompting one to confirm which parameter is being measured. In this case make sure it says 'Power' and press the 'OK' button on the bottom right of the window before continuing.

The final configuration step for the Z-Scan data collection process will be managed in the 'Settings' menu on the right side of the 'Monitoring' tab. Follow the settings in Fig. 14(b) for the Z-Scan. Make sure to change the 'File Path' to an appropriate folder. Before each Z-Scan make sure to change the 'File Name' so that the data from a previous Z-Scan is not overwritten. Double-Check to make sure there are 171 Samples and the 'Number

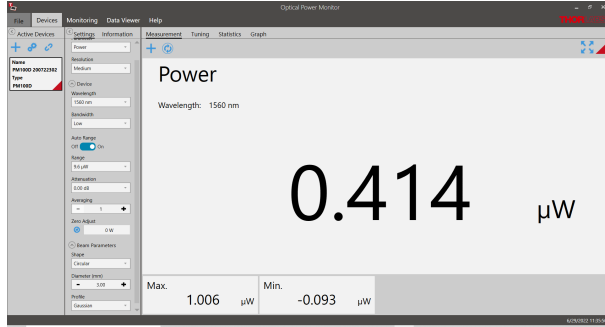


(a) Closed-aperture Z-Scan.

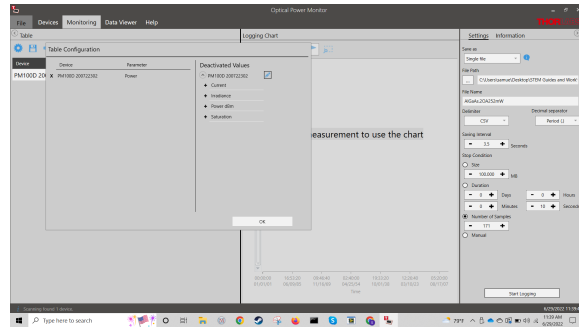


(b) Connecting the power meter to a laptop with USB cable.

Figure 13.



(a) Under 'Beam Parameters', set the profile to 'Gaussian'



(b) Setting 'Device Parameter' to 'Power' and Data Collection Settings.

Figure 14.

of Samples' selection dot is marked. Lastly, adjust the 'Saving Interval' to a time-frame that is comfortable (3-5 seconds is recommended). Before starting each scan, ensure that the sample's translation stage is set to the zero marker.



(a)



(b)

Figure 15. (a) Translation stage set to the zero marker. (b) Translation stage moved ten ticks.

When fully prepared for the Z-Scan to start, press the 'Start Logging' button. Upon pressing this button, the system will immediately begin taking measurements. One will have the 'Saving Interval' time-frame to move the translation stage in increments of 10 on the adjustment knob (note that each small tick on the knob is 0.01 mm, so moving by ten of those ticks for each measurement step is a movement of 0.1 mm or 100 μm for the sample). Remember that this translation stage utilizes gears inside the turning mechanism. Be careful to turn the adjustment knob precisely in units of 10 ticks and to not overshoot the ticks, re-adjusting after overturning the ticks can lead to inaccurate step distance increments in the recorded data. Once the Z-Scan is complete there will be 171 recorded measurements automatically saved into an Excel spreadsheet at the location of the preset file path. After completing a closed-aperture Z-Scan, reset the translation stage to the zero marker and open the adjustable iris aperture.

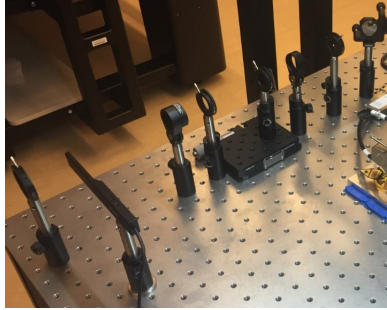


Figure 16. Open Aperture Z-Scan Set-up.

The power-meter must now be moved to a position close to the focal point of the post-sample lens for measurement of the open-aperture Z-Scan. The post-sample lens is just used to ensure that all the optical power of the expanded beam is captured by the sensitive area of the photodetector. Follow the same procedures for the closed-aperture Z-Scan for the open-aperture Z-Scan, ensuring that the ‘File Name’ has been modified as to not overwrite the previous scan data. Once the open-aperture Z-Scan is complete, follow the Pre-Measurement procedures to reset the iris aperture size and then adjust the laser power level with the half-wave plate for another desired power level to continue with a Z-Scan power sweep.

### A.3.6 Post-measurement Procedures

Having collected the (OA and CA) Z-scan measurements, for different incident power levels, save all data in a single CSV file, and use the data processing program<sup>26</sup> to extract the nonlinear parameters. Check section B for more information on the parameter extraction process, and check the software user manual in the software repository<sup>26</sup> to correctly launch the program.

## A.4 ANALYSIS

Having finished the experimental procedures, complete and answer the following tasks and questions.

1. Complete the table with the results obtained from the parameter extraction step.

Table 3. Material and setup parameters

Studied material	(i) $\beta_{TPA}$	(ii) $n_2$	(iii) $w_0$	(iv) a

2. Look for published values of  $\beta_{TPA}$  and  $n_2$  of the studied material in the academic literature (if available, for the used wavelength), and compare them with the results obtained with the experimental practice.
3. Calculate the error percentage (assuming that the published data are the conventionally accepted values), and determine if the results obtained with the experimental practice are reasonable results. Determine possible causes of the obtained error, and suggest ways of improving the experimental or numerical procedures in order to get a lower error value.
4. Closed-aperture measurements carry information about both the  $\beta_{TPA}$  and  $n_2$ , so would it be possible to carry out the Z-scan technique without the open-aperture measurements?
5. To optimize the experimental protocol, how could you reform the optical setup to acquire simultaneously the open-aperture and closed-aperture measurements?
6. If a precise translation stage was not available, but the blocking element had the functionality of precisely tuning the aperture size, would it be possible to conceive a different nonlinear characterization technique to obtain the  $\beta_{TPA}$  and  $n_2$  parameters?

## APPENDIX B. DATA PROCESSING AND PARAMETERS EXTRACTION

An open-source software has been developed for extracting the nonlinear properties, and some setup parameters, from experimental data (like the laboratory measurements illustrated in Fig. 17). It can be accessed from the repository of Ref. 26. The instructions to correctly launch the program are also available in the online repository.

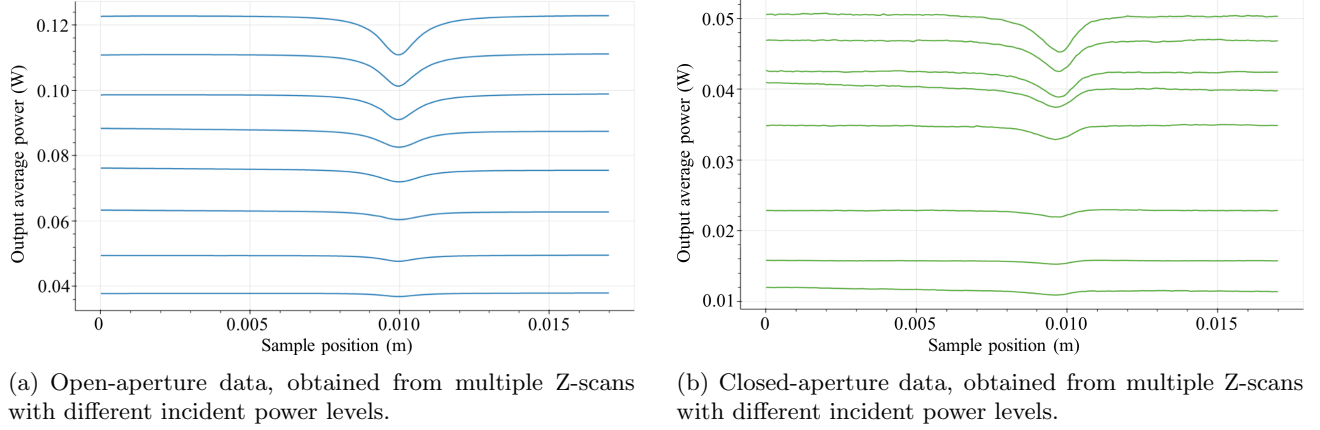


Figure 17. Experimental data obtained from open-aperture and closed-aperture Z-scan measurements, carried out in the  $z$  interval from 0 to 17 mm, for incident average power values between 38 and 123 mW, with a silicon sample with a width of 350  $\mu\text{m}$ , using a pulsed laser source with a pulse duration of 90 fs and a repetition rate of 100 MHz. A power sweep comprising eight incident power levels was performed to enrich the data used to extract the nonlinear properties of the material and some setup parameters.

This software harnesses the analytical model derived and explained in section A.2 for experimental data processing and parameters extraction via numerical propagation methods and curve fitting. It takes as input data, the raw measurements of open-aperture and closed-aperture Z-scans, for different incident power levels. Performing a power sweep, instead of just carrying out a single Z-scan, helps to improve the accuracy of the nonlinear and optical setup parameters estimation. The numerical methodologies implemented for processing open-aperture data and closed-aperture data are different, and they are detailed below.

### B.1 OPEN-APERTURE STUDY

Optical power measurements for the open-aperture setup configuration do not depend on the position of the detection plane, as propagation between the sample and the photodetector do not influence the open-aperture measurement. Therefore, the data processing can be performed directly using Eq. (46), which states the relation between the optical power before and after the sample. By carrying out a numerical fitting of the experimental data, using this analytical model, light beam's  $w_0$  and sample material's  $\beta_{TPA}$  may be inferred. The measurement of  $w_0$  is not required for determining  $\beta_{TPA}$  from the power sweep data, but it is necessary for the accurate estimation of  $n_2$  later on.

For carrying out the processing, a fitting parameter  $F(z)$  is defined as

$$F(z) = \frac{2\beta_{TPA}L_{eff}}{\tau f_{rep} \lambda_0 z_0 \left(1 + \frac{z^2}{z_0^2}\right)} = \left(\frac{2\beta_{TPA}L_{eff}}{\tau f_{rep} \lambda_0}\right) \frac{z_0}{z^2 + z_0^2} = \left(\frac{2\beta_{TPA}L_{eff}}{\tau f_{rep} \lambda_0}\right) \frac{z_0}{(z' - \bar{z})^2 + z_0^2}, \quad (48)$$

preserving the notation introduced in section A.2, and introducing the variables  $z'$  and  $\bar{z}$  in order to make the expression more general, for supporting  $z$ -axis distance measurements not referenced with respect to the focus of the beam. Thus, taking into consideration the definition of  $z_0$  (Eq. (26)), it is possible to reduce Eq. (46) to the expression

$$\bar{P}_{out} = e^{-\alpha_0 L} \frac{1}{F(z)} \ln [1 + F(z)\bar{P}_{in}]. \quad (49)$$

It is relevant to remark that the parameter  $F(z)$  has a lorentzian functional dependence on  $z$ , and it has been written in a lorentzian canonical form in Eq. (48).

The data processing software<sup>26</sup> offers three different methods for determining  $w_0$  and  $\beta_{TPA}$ . It is convenient to test which is more suitable for the available data; since their relative accuracy varies depending on the precision degree of the measurements and the experimental data sampling.

### B.1.1 Logarithmic function-based fitting

The first method comprises an exact logarithmic fitting, directly applying Eq. (49). Thereby, no data standardization is required. A  $\bar{P}_{out}$  vs  $\bar{P}_{in}$  curve is obtained for every  $z$  coordinate, by extracting the corresponding measurement of every Z-scan made in the input power sweep. So, every  $\bar{P}_{out}$  vs  $\bar{P}_{in}$  curve has as many points as incident power levels were tested. Then, leveraging an optimization fitting function, it is possible to find the corresponding value of  $F$  for every  $z$  coordinate of the scans, which provides a numerical description of the  $F(z)$  function associated to the setup under consideration. Having this information, it only remains to perform a lorentzian fitting of  $F(z)$ ; which yields the values for the lorentzian amplitude-related value  $A$ , half-width at half-maximum  $\sigma$ , and center value  $\mu$ . These values have a direct relationship with the parameters involved in the analytical definition of  $F(z)$ . So, by comparing Eq. (48) with the canonical form of a lorentzian function, one gets

$$F(z) = \frac{A}{\pi} \frac{\sigma}{(z' - \mu)^2 + \sigma^2} \rightarrow A = \frac{2\pi}{\lambda_0} \frac{\beta_{TPA} L_{eff}}{\tau f_{rep}}, \quad \sigma = z_0, \quad \mu = \bar{z}; \quad (50)$$

from which it is immediately obtained that

$$w_0 = \sqrt{\frac{\lambda_0 \sigma}{\pi}} \quad \text{and} \quad \beta_{TPA} = \frac{\lambda_0 \tau f_{rep}}{2\pi L_{eff}} A. \quad (51)$$

### B.1.2 Taylor expansion-based fitting

The remaining two methods use a series expansion to represent the logarithmic function in Eq. (49). This allows the use of less sophisticated fitting software, and may provide more stable fittings for experimental measurements with a small number of Z-scans (i.e., power sweep performed for few incident power values).

Thus, using the Maclaurin power series for the analytical function  $\ln[1+x]$ , and considering the first two terms of the expansion, it is possible to find a polynomial expression to approximate the relation between the incident optical power  $\bar{P}_{in}$  and outgoing optical power  $\bar{P}_{out}$ . Using this strategy it is found that

$$\ln[1+x] = \sum_{n=1}^{\infty} \frac{(-1)^{n-1}}{n} x^n \approx x - \frac{1}{2} x^2 \rightarrow \bar{P}_{out} \approx \frac{e^{-\alpha_0 L}}{F(z)} \left( F(z) \bar{P}_{in} - \frac{F^2(z) \bar{P}_{in}^2}{2} \right). \quad (52)$$

Then, one could either find  $F(z)$  performing a linear regression of the ratio  $\bar{P}_{out}/\bar{P}_{in}$  vs  $\bar{P}_{in}$  curve for each  $z$  coordinate, in a similar way as it was done in section B.1.1, or directly solving Eq. (52) for  $F(z)$  and analyzing the resulting lorentzian for every incident power level within the experimental power sweep. These are regarded as the second and third fitting methods. Each of these entails a different way of standardizing data before proceeding with the fitting.

For the second method, the linear regression is performed after having adjusted experimental data according to the expression

$$\frac{1}{e^{-\alpha_0 L} \bar{P}_{in}} \bar{P}_{out} \approx 1 - \frac{F(z)}{2} \bar{P}_{in}; \quad (53)$$

which means that measured output data must get divided by the constant  $e^{-\alpha_0 L}$  and the corresponding incident power value  $\bar{P}_{in}$ , and with this standardized data set a new  $\bar{P}_{in}$ -dependent curve is obtained for every  $z$  coordinate

of the performed Z-scans. The slopes  $a(z)$  of all the calculated linear regressions would store the information required to numerically determine  $F(z)$ , given that

$$1 - \frac{F(z)}{2} \bar{P}_{in} = a(z) \bar{P}_{in} + b(z) \rightarrow F(z) = -2a(z). \quad (54)$$

$b(z)$  is the set of intercepts obtained with the linear regression applied for every  $z$  coordinate. Eq. (54) predicts that they are all values expected to be close to 1.

Having the numerical description of the  $F(z)$  function associated to the setup under consideration, it is possible to perform a second lorentzian fitting and extract  $w_0$  and  $\beta_{TPA}$ , following the same procedure used in section B.1.1.

For the third method, data standardization is made according to the expression

$$\frac{-2}{e^{-\alpha_0 L} \bar{P}_{in}^2} \bar{P}_{out} + \frac{2}{\bar{P}_{in}} = F(z). \quad (55)$$

In this case, the first fitting to obtain  $F(z)$  is not required, since standardizing data as shown in Eq. (55) enables to immediately obtain the numerical description of the  $F(z)$ . If this standardization is applied to data for every incident power level, it is possible to apply a different lorentzian fitting for every standardized data set: one per incident power level considered in the power sweep. So, following the same procedure used in section B.1.1, every lorentzian fitting would provide different pair of values for  $w_0$  and  $\beta_{TPA}$ . All of them are averaged in order to improve method's robustness, and return the final estimations for  $w_0$  and  $\beta_{TPA}$ .

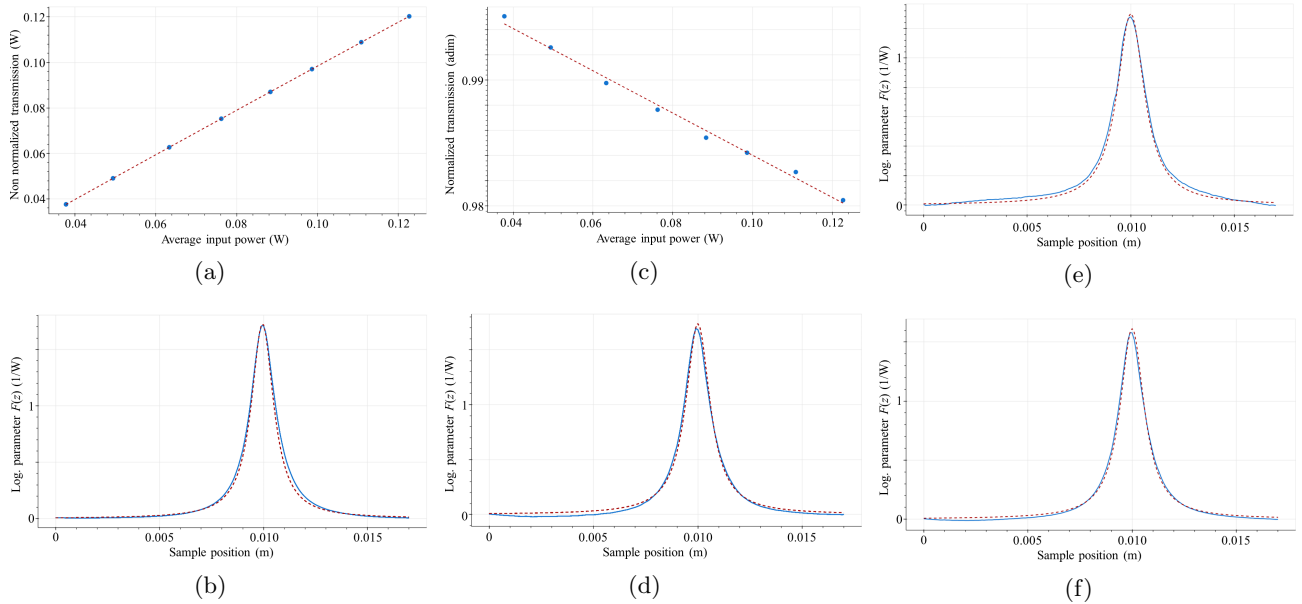


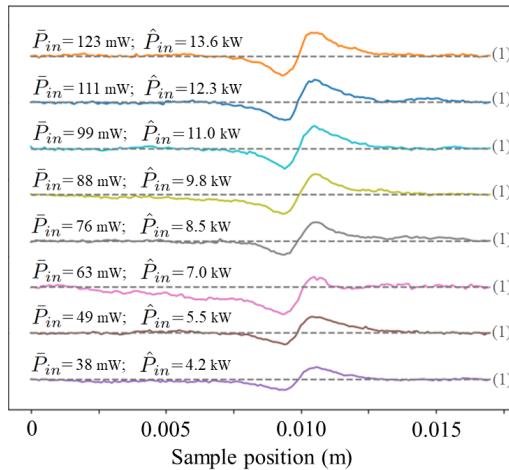
Figure 18. Illustrative curves of the open-aperture fitting methods, applied to the measurement data set from Fig. 17. All solid blue and dashed red plots correspond to experimental and fitting curves, respectively. (a) Example of an exact logarithmic fitting, for the  $\bar{P}_{out}$  vs  $\bar{P}_{in}$  curve evaluated for  $z = 0.0085$  m. (b) Lorentzian second fitting of the numerical description of  $F(z)$ , obtained following the first fitting method. (c) Example of a linear regression fitting, for the standardized  $\bar{P}_{out}/\bar{P}_{in}$  vs  $\bar{P}_{in}$  curve evaluated for  $z = 0.0085$  m. (d) Lorentzian second fitting of the numerical description of  $F(z)$ , obtained following the second fitting method. (e-f) Examples of the lorentzian fittings of the standardized data, according to Eq. (55), for two of the incident power levels considered in the power sweep: 63 mW and 111 mW.

## B.2 CLOSED-APERTURE STUDY

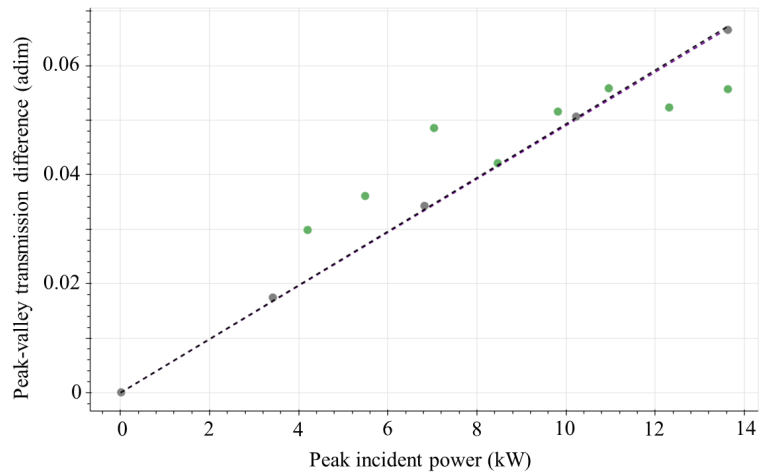
Closed-aperture measurements are made to probe the refractive effects introduced by the nonlinear sample in the incident laser beam. Consequently, it is necessary to model not only the electric field complex amplitude profile of the beam at sample's output facet plane, but also at the aperture plane. Which entails the description of the spatial evolution of the beam affected by the irradiance-dependent phase-shift variation  $\Delta\phi$ . To do this analytically, it is possible to follow different methodologies, such as the Gaussian Decomposition implemented in Ref. 21. In this case, for the developed data processing software,<sup>26</sup> Fourier optics is used to model the propagation, making use of the discrete Fourier transform.

Preferring this numerical methodology implies that it is not possible to directly fit experimental data with a condensed analytical expression; alternatively an optimization software routine was defined, in order to repeatedly perform simulations of the Z-scans for different values of  $n_2$  until the simulation matches the experimental observation.

To follow this optimization approach, it is necessary to determine a targeted value, towards which the optimization routine is expected to converge. This value is calculated using the closed-aperture normalized data. The normalization of closed-aperture data not only involves to scale each Z-scan measurement with respect to the optical transmission value obtained at the linear regime of the scan, so that all normalized curves tend asymptotically to 1 for low and high values of  $z$ . This normalization also requires the subtraction of the non-linear absorption effects, to obtain a set of curves whose features are only related to the nonlinear refraction. Thereby it is necessary to find the quotient between the scaled open-aperture curve and its corresponding scaled closed-aperture curve. Thus, the normalized version of the closed-aperture measurements shown in Fig. 17(b) is presented in Fig.19(a). An offset has been introduced between them to facilitate their visualization, preserving the same scale for all.



(a) Normalized experimental closed-aperture curves, obtained as the quotient between the scaled closed-aperture and open-aperture curves. All curves share the same vertical axis scale, and tend asymptotically to 1 (marked by the dashed gray lines). An offset of 0.05 has been introduced between adjacent curves. Corresponding incident average and peak power values,  $\bar{P}_{in}$  and  $\hat{P}_{in}$ , are indicated.



(b) Superimposed scatter plot of the experimental (green dots) and simulated (gray dots) peak-valley transmission difference  $\Delta T_{p-v}$  obtained from Z-scans with different incident power levels. The slope  $\Delta T'_{p-v}$  of the linear dependence between peak-valley transmission difference and incident optical power is determined by calculating linear regressions (with intercept at the origin) for the experimental (dashed purple line) and simulated (black dashed line) data.

Figure 19. Closed-aperture experimental data normalization and processing.

Curves in Fig. 19(a) have been arranged from the lower positions to the higher ones in order of increasing incident power, so it is possible to notice that as incident power increases, the peak-valley transmission difference  $\Delta T_{p-v}$  increases as well; which is defined as

$$\Delta T_{p-v} = \max\{\bar{P}(z)\} - \min\{\bar{P}(z)\}, \quad (56)$$

where  $\bar{P}$  stands for the normalized optical power detection after the aperture (normalized closed-aperture signal).

As the peak-valley transmission difference varies along with the incident power level, it may be understood as a function of input power; i.e.,  $\Delta T_{p-v} = \Delta T_{p-v}(\bar{P}_{in})$ . And the derivative of this function, which has a linear functional form,<sup>21</sup> is an indicator of how strong the nonlinear refractive response of the material is (i.e., how large is its nonlinear refractive index  $n_2$ ). In this way, the derivative of the peak-valley transmission difference with respect to the incident power level  $\Delta T'_{p-v}(\bar{P}_{in})$  is set as the quantity to extract from the experimental closed-aperture data, and use as the numerical optimization target. In the software, this is made by applying a linear regression on the set of experimental  $\Delta T_{p-v}$  values. Fig. 19(b) shows, as green scattered dots, the  $T_{p-v}$  values associated to the normalized closed-aperture measurements, and the purple dashed line is the linear function used to estimate the slope  $\Delta T'_{p-v}(\bar{P}_{in})$  that corresponds to the sample under study. It is evident the convenience of performing a power sweep, for different incident power levels, instead of just performing a single Z-scan: random experimental errors get mitigated, and the general trend may be extracted from the measurements cluster.

Having a target value defined, the optimization routine is executed. Many Z-scans are numerically simulated for different  $\bar{P}_{in}$  values. Each of these simulated Z-scans implies the numerical propagation and detection of the modeled optical power for different  $z$  positions of the sample. Each numerical propagation is calculated using the corresponding Fourier optics transform method, so that the electric field's complex amplitude profile at the aperture plane  $E_a$  would be given by

$$E_a = e^{ik_0\Delta z} \mathcal{F}^{-1}\{ e^{-i\pi\lambda_0\Delta z(k_x^2+k_y^2)} \mathcal{F}\{ E(\ell=L) \} \} \quad (57)$$

where  $\mathcal{F}$  stands for the two-dimensional Fourier transform,  $k_x$  and  $k_y$  are the  $x$  and  $y$  components of the  $k$ -vector in the spatial frequency domain, and  $\Delta z$  is the distance to propagate from the sample's output facet plane to the aperture plane, which is adjusted properly during each Z-scan simulation (see Figs. 20(a-d)). Each detection is carried out by integrating numerically the irradiance profile, calculated from the electric field's complex amplitude profile at the aperture plane. Whereas in the physical optical system there is a gap between the aperture and the photodetector, the numerical integration is directly performed for the field at the aperture plane because the short propagation between the aperture and the photodetector does not introduce any variation in the optical power detection. The simulated open-aperture detection is performed for the entire beam profile at the aperture plane. For the closed-aperture simulations, a Heaviside function (in polar coordinates) is used to make zero the field profile distribution for coordinates outside of a circle with radius  $a$ ; which introduces the effect of the physical aperture (see Figs. 20(e-f)).

The simulated power sweep is then performed for different values of  $n_2$ . From each power sweep, a different  $\Delta T'_{p-v}(\bar{P}_{in})$  slope value is calculated (using another linear regression). The optimization routine keeps running until a the error percentage between the simulated and experimental  $\Delta T'_{p-v}$  values is below a tolerance threshold. The  $n_2$  associated with this low error percentage is the one reported as the estimated  $n_2$ . The results of such optimization are presented in Fig. 19(b), which shows as gray scattered dots the simulated values of the power sweep with the optimized  $n_2$  value, and the dashed gray line is the fitted linear function for the slope extraction. It is clear from the figure that the optimization obtained an estimation for  $n_2$  that produce a  $\Delta T_{p-v}$  variation comparable with the one measured experimentally, since the slopes  $\Delta T'_{p-v}$  of the experimental and simulated datasets are almost identical.

Finally, it is relevant to annotate that the software<sup>26</sup> also provides a mechanism for indirectly estimating the size of the aperture used in the experimental closed-aperture Z-scans. For this aim another optimization routine is employed. From the experimental data provided, the software compares the transmitted power between the corresponding closed- and open-aperture Z-scans (in the linear regime). The ratio of the transmission is associated to the size of the aperture, as smaller apertures would allow the transmission of a lower power percentage. The

average of all ratios (one per OA and CA Z-scans pair) is thus used as the targeted value for the optimization routine. Next, the Gaussian beam at the aperture plane is simulated with the user-provided setup parameters, and its irradiance profile is numerically integrated. This is the simulated open-aperture transmission in the linear regime. Then, the profile gets ‘filtered’ with Heaviside functions (in polar coordinates) with different radii values  $a$ , and the remaining power within the corresponding circle is calculated. These are the simulated closed-aperture transmission values in the linear regime, for different simulated apertures. Finally, the ratios between all the calculated closed-aperture values and the reference open-aperture value are obtained, and compared with the experimental target value. The aperture optimization routine keeps running until a the error percentage between the simulated and experimental  $a$  values is below a tolerance threshold. The radius  $a$  associated with the lowest error percentage is the one reported as the numerically estimated  $a$ .

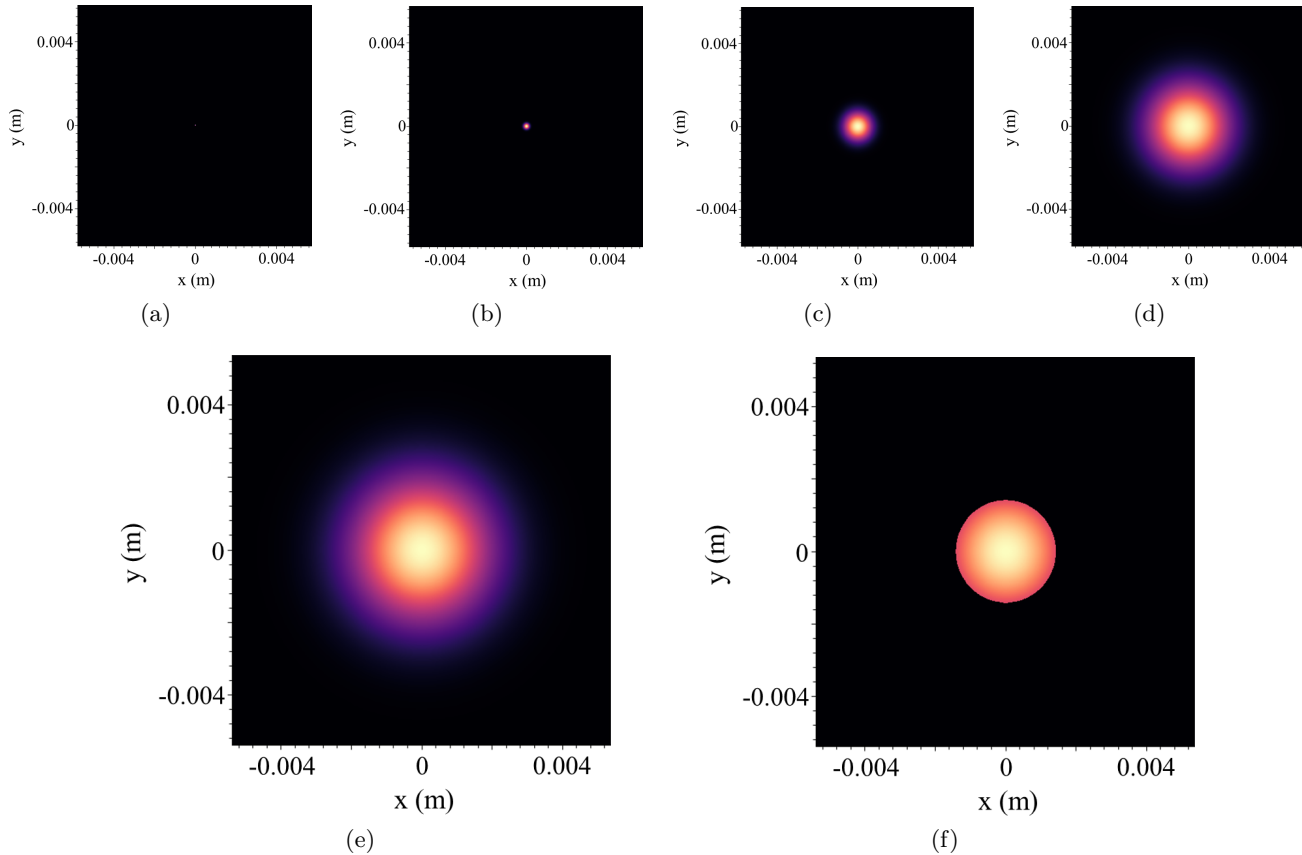


Figure 20. Simulated laser beam cross-section irradiance profiles, obtained from electric field’s complex amplitude profiles, calculated for different planes of the setup. Displayed irradiance profiles do not share color scales, in order to improve the visualization of the figures. (a-d) Illustration of the numerical Fourier transform-based propagation. Irradiance profiles are respectively evaluated at  $z = z_0$ ,  $z = 10 z_0$ ,  $z = 50 z_0$ ,  $z = 150 z_0$ . (e-f) Illustration of the simulated irradiance profiles at the aperture plane, used for open- and close-aperture power calculation. It is evident how the polar Heaviside function is used to simulate the effect of the aperture as blocking element.

### ACKNOWLEDGMENTS

The authors are grateful to Dr. Natalia Múnera, University of Central Florida (CREOL), USA, for fruitful discussions and technical advice provided for the design of the experiments.

## REFERENCES

- [1] Glick, M., Kimmerling, L. C., and Pfahl, R. C., “A roadmap for integrated photonics,” *Optics and Photonics News* **29**(3), 36–41 (2018).
- [2] Minzioni, P., Lacava, C., Tanabe, T., Dong, J., Hu, X., Csaba, G., Porod, W., Singh, G., Willner, A. E., Almainan, A., et al., “Roadmap on all-optical processing,” *Journal of Optics* **21**(6), 063001 (2019).
- [3] Moody, G., Sorger, V. J., Blumenthal, D. J., Juodawlkis, P. W., Loh, W., Sorace-Agaskar, C., Jones, A. E., Balram, K. C., Matthews, J. C., Laing, A., et al., “2022 roadmap on integrated quantum photonics,” *Journal of Physics: Photonics* **4**(1), 012501 (2022).
- [4] Pelucchi, E., Fagas, G., Aharonovich, I., Englund, D., Figueroa, E., Gong, Q., Hannes, H., Liu, J., Lu, C.-Y., Matsuda, N., et al., “The potential and global outlook of integrated photonics for quantum technologies,” *Nature Reviews Physics* **4**(3), 194–208 (2022).
- [5] Metcalf, B. J., Spring, J. B., Humphreys, P. C., Thomas-Peter, N., Barbieri, M., Kolthammer, W. S., Jin, X.-M., Langford, N. K., Kundys, D., Gates, J. C., et al., “Quantum teleportation on a photonic chip,” *Nature photonics* **8**(10), 770–774 (2014).
- [6] Spring, J. B., Metcalf, B. J., Humphreys, P. C., Kolthammer, W. S., Jin, X.-M., Barbieri, M., Datta, A., Thomas-Peter, N., Langford, N. K., Kundys, D., et al., “Boson sampling on a photonic chip,” *Science* **339**(6121), 798–801 (2013).
- [7] Moille, G., Combrié, S., Morgenroth, L., Lehoucq, G., Neuilly, F., Hu, B., Decoster, D., and de Rossi, A., “Integrated all-optical switch with 10 ps time resolution enabled by ald,” *Laser & Photonics Reviews* **10**(3), 409–419 (2016).
- [8] Hu, X.-M., Zhang, C., Liu, B.-H., Cai, Y., Ye, X.-J., Guo, Y., Xing, W.-B., Huang, C.-X., Huang, Y.-F., Li, C.-F., et al., “Experimental high-dimensional quantum teleportation,” *Physical Review Letters* **125**(23), 230501 (2020).
- [9] Gómez, E. S., Gómez, S., González, P., Cañas, G., Barra, J. F., Delgado, A., Xavier, G. B., Cabello, A., Kleinmann, M., Vértesi, T., et al., “Device-independent certification of a nonprojective qubit measurement,” *Physical review letters* **117**(26), 260401 (2016).
- [10] Martínez, D., Tavakoli, A., Casanova, M., Canas, G., Marques, B., and Lima, G., “High-dimensional quantum communication complexity beyond strategies based on bell’s theorem,” *Physical review letters* **121**(15), 150504 (2018).
- [11] Manufacturing USA, “Aim photonics (american institute for manufacturing integrated photonics).” <https://www.manufacturingusa.com/institutes/aim-photonics> (2022). Accessed: 26 July 2022.
- [12] “National photonics initiative.” <https://www.lightourfuture.org/home/> (2022). Accessed: 26 July 2022.
- [13] Hecht, Jeff, “Industrializing photonics - laser focus world.” <https://www.laserfocusworld.com/optics/article/14203511/industrializing-photonics> (2021). Accessed: 26 July 2022.
- [14] Manufacturing USA, “Attracting stem talent for careers in advanced manufacturing.” <https://www.manufacturingusa.com/studies/attracting-STEM-talent-careers-advanced-manufacturing> (2022). Accessed: 26 July 2022.
- [15] Massachusetts Center for Advanced Manufacturing, “News.” <https://cam.masstech.org/news> (2022). Accessed: 26 July 2022.
- [16] “National quantum initiative.” <https://www.quantum.gov/> (2021). Accessed: 26 July 2022.
- [17] Kirchain, R., Moore, E., Field, F. R., Saini, S., and Westerman, G., “Preparing the advanced manufacturing workforce: A study of occupation and skills demand in the photonics industry,” (Feb 2021).
- [18] Stegeman, G. I. and Seaton, C. T., “Nonlinear integrated optics,” *Journal of applied physics* **58**(12), R57–R78 (1985).
- [19] Garmire, E., “Nonlinear optics in daily life,” *Optics express* **21**(25), 30532–30544 (2013).
- [20] Petrella, J. K. and Jung, A. P., “Undergraduate research: Importance, benefits, and challenges,” *International journal of exercise science* **1**(3), 91 (2008).
- [21] Sheik-Bahae, M., Said, A. A., Wei, T. H., Hagan, D. J., and Stryland, E. V., “Sensitive measurement of optical nonlinearities using a single beam,” *IEEE J. Quantum Electron.* **26**(4), 760–769 (1990).

- [22] Compound Semiconductor, “Building better lasers on low-cost silicon.” [https://compoundsemiconductor.net/article/107444/Building\\_Better\\_Lasers\\_On\\_Low-cost\\_Silicon/feature](https://compoundsemiconductor.net/article/107444/Building_Better_Lasers_On_Low-cost_Silicon/feature) (2019). Accessed: 26 July 2022.
- [23] Photonics Media, “Single-process and inexpensive optical fiber fabrication method will enable self-production.” [https://www.photonics.com/Articles/Single-Process\\_and\\_Inexpensive\\_Optical\\_Fiber/a66164](https://www.photonics.com/Articles/Single-Process_and_Inexpensive_Optical_Fiber/a66164) (2020). Accessed: 26 July 2022.
- [24] Photonics Online, “Newport introduces affordable, compact and simple photonics control devices.” <https://www.photoniconline.com/doc/newport-introduces-affordable-compact-and-0001> (2010). Accessed: 26 July 2022.
- [25] Chapple, P., Staromlynska, J., and McDuff, R., “Z-scan studies in the thin-and the thick-sample limits,” *JOSA B* **11**(6), 975–982 (1994).
- [26] Arango, J. J., “Z-scan: Parameter extraction program.” <https://github.com/juanjosearango/z-scan-parameter-extraction-program> (2022). Accessed: 26 July 2022.
- [27] Zhang, L., Agarwal, A. M., Kimerling, L. C., and Michel, J., “Nonlinear group IV photonics based on silicon and germanium: from near-infrared to mid-infrared,” *Nanophotonics* **3**(4-5), 247–268 (2014).
- [28] Boyd, R. W., [*Nonlinear optics*], Academic Press (2020).
- [29] Agrawal, G. P., “Nonlinear fiber optics,” in [*Nonlinear Science at the Dawn of the 21st Century*], 195–211, Springer (2000).
- [30] Mizuguchi, T. and Nuriya, M., “Applications of second harmonic generation (SHG)/sum-frequency generation (SFG) imaging for biophysical characterization of the plasma membrane,” *Biophysical Reviews* **12**(6), 1321–1329 (2020).
- [31] Kumar, V., Coluccelli, N., and Polli, D., “Chapter 5 - coherent optical spectroscopy/microscopy and applications,” in [*Molecular and Laser Spectroscopy*], Gupta, V., ed., 87–115, Elsevier (2018).
- [32] Couteau, C., “Spontaneous parametric down-conversion,” *Contemporary Physics* **59**(3), 291–304 (2018).
- [33] Keller, T. E. and Rubin, M. H., “Theory of two-photon entanglement for spontaneous parametric down-conversion driven by a narrow pump pulse,” *Physical Review A* **56**(2), 1534 (1997).
- [34] Hill, K., Johnson, D., Kawasaki, B., and MacDonald, R., “CW three-wave mixing in single-mode optical fibers,” *Journal of Applied Physics* **49**(10), 5098–5106 (1978).
- [35] Anwar, A., Perumangatt, C., Steinlechner, F., Jennewein, T., and Ling, A., “Entangled photon-pair sources based on three-wave mixing in bulk crystals,” *Review of Scientific Instruments* **92**(4), 041101 (2021).
- [36] Dudley, J. M., Genty, G., and Coen, S., “Supercontinuum generation in photonic crystal fiber,” *Reviews of modern physics* **78**(4), 1135 (2006).
- [37] Dudley, J. M. and Taylor, J. R., [*Supercontinuum generation in optical fibers*], Cambridge University Press (2010).
- [38] Dashtban, Z., Salehi, M. R., and Abiri, E., “Supercontinuum generation in near-and mid-infrared spectral region using highly nonlinear silicon-core photonic crystal fiber for sensing applications,” *Photonics and Nanostructures-Fundamentals and Applications* **46**, 100942 (2021).
- [39] Poudel, C. and Kaminski, C. F., “Supercontinuum radiation in fluorescence microscopy and biomedical imaging applications,” *JOSA B* **36**(2), A139–A153 (2019).
- [40] Brosnan, S. and Byer, R., “Optical parametric oscillator threshold and linewidth studies,” *IEEE Journal of Quantum Electronics* **15**(6), 415–431 (1979).
- [41] Barbier, M., Zaquine, I., and Delaye, P., “Generation of correlated photon pairs by spontaneous four-wave mixing in liquid-core microstructured fibres,” in [*2014 The European Conference on Optical Communication (ECOC)*], 1–3, IEEE (2014).
- [42] Fisher, R. A., [*Optical phase conjugation*], Academic press (2012).
- [43] Saleh, B. E. and Teich, M. C., [*Fundamentals of photonics*], John Wiley & sons (2019).
- [44] Sheik-Bahae, M., Said, A. A., and Stryland, E. W. V., “High-sensitivity, single-beam n<sup>2</sup> measurements,” *Opt. Lett.* **14**(17), 955–957 (1989).